Reducing fuel consumption and related emissions through optimal sizing of energy storage systems for diesel-electric trains

Marko Kapetanović [a,*], Alfredo Núñez [b], Niels van Oort [a], Rob M.P. Goverde [a]

[a] Department of Transport and Planning, Delft University of Technology, P.O. Box 5048, 2600 GA Delft, the Netherlands
[b] Section of Railway Engineering, Delft University of Technology, P.O. Box 5048, 2600 GA Delft, the Netherlands

HIGHLIGHTS

- Optimal Lithium-ion battery sizing for hybrid diesel-electric train is presented.
- Bi-level optimization approach integrates optimal sizing and control levels.
- Two energy management strategies are developed and compared.
- Trade-off between fuel savings and hybridization cost is analyzed.
- Fuel savings and CO_2 emissions reduction of up to 34.5% is obtained.

ARTICLE INFO

ABSTRACT

Hybridization of diesel multiple unit railway vehicles is an effective approach to reduce fuel consumption and related emissions in regional non-electrified networks. This paper is part of a bigger project realized in collaboration with Arriva, the largest regional railway undertaking in the Netherlands, to identify optimal solutions in improving trains' energy and environmental performance. A significant problem in vehicle hybridization is determining the optimal size for the energy storage system, while incorporating an energy management strategy as well as technical and operational requirements. With the primary requirement imposed by the railway undertaking to achieve emission-free and noise-free operation within railway stations, we formalize this as a bi-level multi-objective optimization problem, including vehicle performance, the trade-off between fuel savings and hybridization cost, influence of the energy management strategy, and other constraints. By deriving a Li-ion battery parameters at the cell level, a nested coordination framework is employed, where a brute force search finds the optimal battery size using dynamic programming for full controller optimization for each feasible solution. In this way, the global minimum for fuel consumption for each battery configuration is achieved. The results from a Dutch case study demonstrated fuel savings and CO_2 emission reduction of more than 34% compared to a standard vehicle. Additionally, benefits in terms of local pollutants (NO_x and PM) emissions are observed. Using an alternative sub-optimal rule-based control demonstrated a significant impact of the energy management on the results, reflected in higher fuel consumption and increased battery size together with corresponding costs.

1. Introduction

Air pollution is of great concern in politics, the scientific community, industry, and society in general. The global warming effect caused by greenhouse gasses (GHG) and especially carbon dioxide (CO_2) emissions from anthropogenic sources led to various international treaties, such as the Kyoto Protocol [1] and the follow-up Paris Agreement [2], resulting in recommendations and defined targets to reduce the emissions. Particularly, the transport sector is one of the most significant contributors to GHG emissions and therefore targets have been defined for transportation systems at all levels. In the case of the railway sector, targets were set in 2008 by the International Union of Railways (UIC) and the Community of European Railway and Infrastructure Companies

---

Nomenclature

Abbreviations

AC	alternating current
ATS	after-treatment system
BEMU	battery-electric multiple unit
CER	Community of European Railway and Infrastructure Companies
CO_2	carbon dioxide
DC	direct current
DE	diesel-electric
DHD	diesel-hydrodynamic
DHM	diesel-hydromechanic
DLC	double layer capacitor
DMU	diesel multiple unit
DP	dynamic programming
DPF	diesel particulate filter
EFCM	equivalent fuel consumption minimization
EGR	exhaust gas recirculation
EM	electric motor
EMR	energetic macroscopic representation
EMS	energy management strategy
EMU	electric multiple unit
EoL	end-of-life
ESS	energy storage system
EV	electric vehicle
FCMU	fuel cell multiple unit
G	generator
GHG	greenhouse gasses
ICE	internal combustion engine
NO_x	nitrogen oxides
NRMM	Non-Road Mobile Machinery
PM	particle matter
RB	rule-based
RU	railway undertaking
SCR	selective catalytic reduction
sLFP	super Lithium Iron Phosphate
SoC	state-of-charge
UIC	International Union of Railways

Subscripts/indexes

i	state-of-charge index, $i \in \{1, \cdots, I\}$
j	control variable index, $j \in \{1, \cdots, M\}$
k	time index, $k \in \{0, \cdots, K\}$

Parameters

a_{max}	maximum acceleration $[m/s^2]$
a_{min}	maximum deceleration $[m/s^2]$
$C_{cell,nom}$	nominal capacity of battery cell [As]
d_w	wheel diameter [m]
$E_{elaux,stop,max}$	maximum energy required for supplying electrical auxiliaries during stops [Ws]
$E_{cell,max}$	maximum energy of battery cell [Ws]
g	gravitational acceleration $[m/s^2]$
i_{ag}	constant gear ratio [-]
m_{cell}	mass of battery cell [kg]
$m_{ESS,max}$	maximum allowed battery mass [kg]
m_{pax}	total weight of passengers [kg]
m_{tare}	empty vehicle mass [kg]
m_v	total vehicle mass [kg]
$P_{cell,cont,ch}$	maximum continuous charging power of battery cell [W]
$P_{cell,cont,dch}$	maximum continuous discharging power of battery cell [W]
P_{elaux}	electrical auxiliaries power [W]

$P_{EM,max}$	electric motor maximum power [W]
$P_{ICE,max}$	scaled internal combustion engine maximum power [W]
$P_{ICE,max0}$	original internal combustion engine maximum power used in scaling [W]
p_{maux}	ratio of the internal combustion engine output power used for mechanical auxiliaries [-]
R_{cell}	internal resistance of battery cell $[\Omega]$
$R_{cell,ch}$	internal battery cell resistance during charging $[\Omega]$
$R_{cell,dch}$	internal battery cell resistance during discharging $[\Omega]$
r_0	Davis equation coefficient (constant term) [N]
r_1	Davis equation coefficient (linear term) $[N/(m/s)]$
r_2	Davis equation coefficient (quadratic term) $\left[N/(m/s)^2\right]$
S_v	vehicle cross-sectional surface $[m^2]$
T	total trip duration [s]
$T_{EM,max}$	maximum torque of the electric motor [Nm]
$T_{G,max}$	maximum torque of the generator [Nm]
$U_{cell,max}$	maximum voltage of battery cell [V]
$U_{cell,min}$	minimum voltage of battery cell [V]
v_{max}	maximum velocity [m/s]
ε_{CO2}	CO_2 emission factor [kg/l]
η_{ag}	axle gear efficiency [-]
λ	rotating mass factor [-]
ρ	fuel density [kg/l]
σ_{max}	maximum battery state-of-charge [-]
σ_{min}	minimum battery state-of-charge [-]
$\sigma_{min,run}$	battery state-of-charge lower limit during motion [-]
$\sigma_{min,stop}$	battery state-of-charge lower limit during stops [-]
σ_{nom}	nominal battery state-of-charge [-]
$\omega_{EM,max}$	maximum rotational speed of the electrical motor [rad/s]
$\omega_{G,max}$	maximum rotational speed of the generator [rad/s]
$\omega_{w,max}$	maximum rotational speed of the wheel [rad/s]

Dynamic variables

a	vehicle acceleration $[m/s^2]$
B	total fuel consumption [l]
B^*	optimal cost-to-go
B_π	total cost-to-go of applying control policy π
$C_{ESS,nom}$	battery nominal capacity [As]
C_0	Willans lines approximation coefficient $[kg\,(Ws)^{-1}]$
C_1	Willans lines approximation coefficient $[kg\,(Ws)^{-1}\,(Nm)^{-1}]$
C_2	Willans lines approximation coefficient $[kg\,(Ws)^{-1}\,(Nm)^{-2}]$
E_{CO2}	total CO_2 emissions [kg]
E_{NOx}	total NO_x emissions [kg]
E_{PM}	total PM emissions [kg]
f_k	transition cost function f_k defined as the fuel consumption during one step
f_K	terminal cost function for the resulting state in the last stage of the horizon
F_w	tractive/braking effort at the wheel [N]
I_{cell}	battery cell current [A]
I_{ESS}	battery current [A]
J	objective function (weighted sum of fuel consumption and hybridization cost) [-]
J_1	lowest possible fuel consumption [l]
J_1^{nom}	nominal (largest possible) value of J_1 [l]
J_2	hybridization cost [EUR]
J_2^{nom}	nominal (largest possible) value of J_2 [EUR]
l_t	tunnel length [m]
n_{ESS}	battery size, $n_{ESS} = [n_{par}\ n_{ser}]$
n_{ESS}^*	optimal battery size
$N_{ESS}^{feasible}$	set of feasible battery sizes, $N_{ESS}^{feasible} = [n_{par}\ n_{ser}]^S \in \mathbb{Z}^2 \times$

	$\mathbb{Z}^S$	
n_{par}	number of battery parallel branches	
n_{par}^*	optimal number of battery parallel branches	
n_{ser}	number of battery cells per branch	
n_{ser}^*	optimal number of battery cells per branch	
P_{DC}	total requested electrical power at the DC link [W]	
P_{EM}	electrical power of the electric motor [W]	
P_G	mechanical input power of the generator [W]	
P_{ICE}	mechanical output power of the internal combustion engine [W]	
$P_{ICE,G}$	electrical output power of the generator [W]	
R	total resistances [N]	
R_c	curve resistances [N]	
R_{ESS}	battery internal resistance [Ω]	
R_g	grade resistances [N]	
R_l	line resistances [N]	
R_t	tunnel resistances [N]	
R_v	vehicle resistances [N]	
s	distance traveled [m]	
S_{ICE}	scaling factor [-]	
S_t	tunnel cross-sectional surface [m^2]	
t	time [s]	
t_k	discretized time variable, $t_k \in \{t_0, \cdots, t_K\}$ [s]	
T_{EM}	torque at the mechanical output of the electric motor [Nm]	
T_G	torque at the mechanical input of the generator [Nm]	
T_w	torque at the wheel [Nm]	
U_{cell}	battery cell terminal voltage [V]	

U_{ESS}	battery terminal voltage [V]
$U_{ESS,max}$	maxium battery terminal voltage [V]
$U_{ESS,min}$	minimum battery terminal voltage [V]
U_{OC}	battery open circuit voltage [V]
$U_{OC,cell}$	battery cell open-circuit voltage [V]
v	vehicle velocity [m/s]
x	control variable, $x \in [-1, 1]$
x_j	discretized values of the control variable, $x_j \in \{x_1, \cdots, x_M\}$
α	weight representing preference towards lower hybridization cost over lower fuel consumption, $\alpha \in [0, 1]$
γ	track gradient [rad]
ε_{NOx}	NO_x emission rate [kg/s]
ε_{PM}	PM emission rate [kg/s]
η_{EM}	efficiency of the electric motor [-]
η_G	efficiency of the generator [-]
π	control policy, $\pi = \{x(\sigma(t_k), t_k) | k = \{0, \cdots, K-1\}\}$
π^*	optimal control policy
σ	battery state-of-charge, $\sigma \in [\sigma_{min}, \sigma_{max}]$ [-]
σ_i	discretized values of the state variable, $\sigma_i \in \{\sigma_1, \cdots, \sigma_I\}$ [-]
$\sigma_{i,j}$	resulting state obtained by applying the control variable x_j to the state σ_i
ϕ	track curve radius [m]
ψ	specific fuel consumption [kg/Ws]
ω_{EM}	rotational speed of the electric motor [rad/s]
ω_{ICE}	rotational speed of the internal combustion engine [rad/s]
ω_w	rotational speed of the wheel [rad/s]

(CER). A short-term target is to decrease specific average CO_2 emissions by 2020 by 30% compared to the 1990 base year level. Medium and long-term targets are further decreased by 50% in 2030, and carbon-free train operation by 2050 [3]. Additionally, local pollutants such as nitrogen oxides (NO_x) and particle matter (PM) gained increasing attention in the railway community over recent years. This is mainly due to the introduction of the EU Non-Road Mobile Machinery (NRMM) Directive in 2016 to diesel rail vehicles and the application of the Stage IIIB emission limits. Addressing the limits of local pollutants raises significant challenges such as new considerations of vehicle design and manufacturing, reliability of new equipment in terms of produced emissions, and new assessments of life cycle costs, including explicitly the effects of emissions [4].

Emerging automotive powertrain technologies for electric vehicles (EVs) are considered as a viable solution in reducing environmental footprints from the predominant road transport sector [5]. Continuous advancements on propulsion systems for EVs offer flexible design, improved vehicle performance and safety [6]. For the railway sector, synergetic electrification of railway lines [7,8] and an increase of renewable sources in electricity production [9] is recognized as one of the most effective measures in improving energy efficiency and reducing GHG emissions. The share of electrified versus non-electrified railway lines has increased from less than 30% in 1975 to up to more than 60% in 2008 in the EU-28 countries. However, this share remained relatively constant over the years 2008–2015 [10]. High capital investments [11,12] with the significant environmental impact of the electrification process [13] and the emergence of new traction options for railways such as alternative fuels [14] and hybrid propulsion systems [15,16], indicate that non-electrified railways will continue to play an essential role in passengers transport. Hence, there is a constant need to improve their performance in terms of energy efficiency, fuel consumption, and emissions. This especially concerns regional railway networks that are often characterized by non-electrified lines due to high investments required for electrification and a low transport demand (low utilization) compared to the main corridors.

Several emission-free alternatives to diesel multiple units (DMU), as predominant vehicles employed in non-electrified regional transport, are being developed in recent years. Battery-electric multiple units (BEMU) and fuel cell multiple units (FCMU) are identified as suitable long-term solutions [17]. However, existing limitations related to the range, flexibility, supporting infrastructure requirements, as well as techno-economic immaturity of these technologies [18], stipulate further development and exploitation of internal combustion engines (ICE). Beatrice et al. [19] analyzed a number of emerging ICE technologies and exhaust after-treatment systems (ATS) for on-road heavy-duty ICEs that are transferable to the rail sector. The results indicate the great potential of waste heat recovery in improving ICE fuel efficiency. Moreover, combining different ATSs, such as exhaust gas recirculation (EGR), diesel particulate filter (DPF), and selective catalytic reduction (SCR) technologies, can contribute in meeting the most stringent emission requirements imposed for the rail sector [20].

Since previous technologies relate mainly to the introduction of new rolling stock, and having in mind the long cycle life of DMUs reaching up to 30 years, transport companies are seeking suitable transition solutions towards emission-free operation, mainly through improving energy efficiency. As identified in [21], the reduction of energy consumption from railway operation can be achieved in several ways: more energy-efficient rolling stock, minimizing energy consumption of auxiliary systems during stabling periods, optimization of the rolling stock deployment based on capacity and demand, energy-efficient timetabling and energy-efficient train control. This paper focuses on the first two options, in particular on the assessment of potential fuel savings and emissions reduction from hybridization of existing DMU vehicles, that would enable the utilization of regenerated energy, as well as (partial or temporal) electrification of auxiliary systems. Several hybrid railway vehicles from major manufacturers (e.g. Siemens [22], Hitachi [23,24], Alstom [25,26]) being tested or already in service, as well as European research projects (e.g. ULEV-TAP 2 [27], CleanER-D [28], DfTRG/0078/2007 [29,30]), have demonstrated significant benefits reflected in fuel savings up to ~40%, depending on the technology

and operational characteristics.

Focusing on a case study of regional railway services provided by Arriva on the Northern lines in the Netherlands, this paper proposes an integrated optimization of energy storage system (ESS) size and energy management strategy (EMS), considering conventional DMU vehicles from the Dutch network converted to their hybrid counterpart. The primary requirement for the hybridization defined by the railway undertaking (RU) is achieving emission-free and noise-free operation within railway stations by switching off diesel engines and powering auxiliary systems solely by ESS. This especially concerns terminal stations, characterized by extended stabling periods. Expected benefits are reflected in total fuel consumption reduction by utilizing brake energy, an increase of overall ICE efficiency by avoiding low load engine operation, and support for the ICE during high-power demand (acceleration) phases.

1.1. Related work

The reduction of fuel consumption and related emissions of DMUs can be achieved by their hybridization, i.e., by adding an on-board ESS. In this section, we review the literature on rail vehicle hybridization, focusing primarily on passenger diesel-driven vehicles. We will not consider freight locomotives as they represent a different use case, nor catenary-fed vehicles (e.g., trams, electric multiple-units – EMUs) since they are not per definition hybrid vehicles [31]. For a comprehensive overview of different measures for energy consumption reduction in the case of urban rail transportation, readers are referred to [32]. An overview focusing on strategies and ESS technologies for optimal regenerative braking usage in urban rail transportation systems can be found in [33]. We analyze the literature covering the main hybridization aspects, starting from the modeling approaches for hybrid propulsion systems and further investigating different design levels.

Reliable mathematical and simulation models are required to assess potential benefits from hybridization in terms of fuel savings and emissions reduction. Widely used models that can support the assessment of environmental impact in railway operations, such as ARTEMIS [34], EcoTransit [35], or EcoPasssenger [36], calculate the fuel consumption and emissions based on mechanical energy using mostly one-lumped efficiency and fixed fuel consumption and emission factors. These models provide predictions for conventional railway vehicles. The case of hybrid vehicles requires more detailed models that include individual components of the powertrain and their interactions. Hybrid vehicle models based on physical relations between the components of the system can be divided into two categories: forward and backward models [37–39]. Forward simulation models follow the physical power flow in the powertrain, starting from the engine, and then to the transmitted and reflected torque to the wheels. They offer realistic control-oriented modeling by capturing driver input/speed control; however, they are usually very complex and characterized by slow execution time and high computer memory. Backward simulation models consider the reverse power flow by computing the tractive contribution required at the wheels and the order of evaluating the system components backward through the system towards the engine, offering a reliable evaluation of vehicle energy consumption based on drive cycle and detailed vehicle-specific data available beforehand. They are also characterized by fast execution times compared to the forward models [39–41]. Depending on the aim of the study, data availability, and the purpose of the simulation model, the adequate type should be selected. Regarding the hybrid DMU railway vehicles, a forward simulation approach is usually used in assessing the potential fuel savings for different driving strategies and styles [42], while backward simulations are performed using mostly typical speed profiles and duty cycles, c.f. [43–47]. In addition to the previous physical models, the energetic macroscopic representation (EMR) is an effective graphical modeling approach in the systemic description of complex propulsion systems [48]. A recent study [49] demonstrated the effectiveness of

using EMR in reverse engineering of railway vehicles to describe power flows behavior and deriving models for the key propulsion system components, disregarding in-depth knowledge of the train energetic devices and sub-systems. It can be particularly useful in case of lack of detailed vehicle-specific parameters due to, e.g. confidentiality aspects or sub-systems provided by subcontractors, by fitting the energetic behavior of the vehicle with the available test data [50]. Furthermore, the approach can be successfully exploited to perform model-based development of suitable energy management strategies [51].

Vehicles hybridization can be considered a multi-objective design optimization problem, with multiple parameters distributed over multiple levels (topology, technology, size, and control). When this optimization problem is solved sequentially (level by level), it is by definition sub-optimal due to coupled dynamic parameters and non-linear effects [52]. In the case of DMU vehicles, topology level refers to the system architecture in terms of the type of the propulsion system, i.e., diesel-electric (DE), diesel-hydrodynamic (DHD), or diesel-hydromechanical (DHM) [53], which directly influences the way the ESS can be integrated into the system. Comparative assessment of the three propulsion systems in terms of integrating different ESS technologies, both mechanical and electrical [16], indicated that DE systems lead to fewer additional physical components for ESS integration. Compared to the DHD and DHM, the DE system enables relatively simple hybridization by adding a proper ESS directly into the electric power transmission system [54]. Since the electric transmission is the only system currently in use on the Northern lines, we limit the analysis to only this particular case in this paper.

The selection of suitable ESS technology is the next step in the DMU hybridization process. Different ESS technologies have emerged in the transport sector for brake energy harvesting [55]. For railway applications, three technologies are being found to be especially suited: batteries, double-layer capacitors (DLCs), and flywheels [56]. Due to their high energy density (energy per unit of mass), rapid technology development and increasing availability on the market, Li-ion batteries are the most represented ESS technology in hybrid DMU-related literature [15]. Compared to Li-ion batteries, DLCs are characterized by both low energy density and high power density. This makes DLCs suitable in applications aimed at high peak power shaving and maximizing the utilization of regenerative braking energy. Although flywheels offer a number of advantages reflected in fast charging and discharging processes and long life cycle, several drawbacks hinder their extensive use in railway applications, related primarily to safety issues, relatively high weight, and high self-discharge rates [33]. In particular cases, combining the advantages of different technologies, typically Li-ion battery and DLC, in a single hybrid ESS, can bring additional benefits compared to a single-technology ESS [47,57]. Considering the main hybridization requirement in our case – emissions-free and noise-free operation within station areas, characterized by low power demand and high energy required, which sums up over time, Li-ion batteries are considered by the RU as the most suitable ESS technology.

While topology and ESS technology choices in the DMU hybridization process are mainly conditioned to the available DMU fleet and main hybridization requirements, thus making these decisions relatively easy, optimal sizing and control of the ESS are complex tasks, which are in most cases treated separately. Taking into account that oversizing of the ESS might unnecessarily increase total ESS mass and volume, as well as total costs, whereas an undersized ESS might lead to considerable energy waste, a detailed analysis is needed to determine an optimal design, while the sizing method depends upon its main function [33]. In particular, a different approach is required if the main intended function of the ESS is, for instance, supporting auxiliaries during stabling periods, maximizing utilization of braking energy, or converting a DMU to a catenary-free EMU. The need for co-design, i.e. integrating the two design optimization levels, has been addressed in hybridization-related literature in general [58], confirming the importance of co-optimization in achieving the best configurations. A recent study [59] proposed an

advanced co-optimization method for fuel cell hybrid vehicles. The two aspects addressed by this co-optimization method are the design of the powertrain affecting the sizing of the system components, and the control of such systems affecting the performance of the system, leading to a trade-off between performance and system sizing. Determination of the component sizing for the fuel cell-battery hybrid energy system for a locomotive application is presented in [60], with the influence of the EMS on the primary design problem addressed by incorporating the two rule-based controls in the optimization framework using particle swarm optimization. Furthermore, adopting the previous approach in [61], the authors provide a set of alternative solutions with different component sizes, from which a planner can select a solution according to its capital and operational expenditure budgets. Although strong interdependence between the optimal ESS sizing and control levels has been widely recognized and established, most of the studies on hybrid DMU railway vehicles focus only on the optimal control, assuming ESS size given beforehand, or roughly estimated before determining the optimal EMS. As a rare example, simultaneous optimization of hybrid ESS (Li-ion battery and DLC) size and energy management strategy for a DE railway vehicle is presented in [47]. The authors used the frequency management approach based on a low-pass filter coupled with dynamic programming as the optimal control method. The existence of multiple ESS technologies, and the solution approach that considers approximations of mixed-integer and discontinuous variables, in this case, raised significant challenges in terms of computation time and errors.

Optimal control strategies aim at minimizing the fuel and/or energy consumption by managing the power flows of different energy sources in place (e.g., ICE and ESS), in particular by determining the optimal moments for charging/discharging the ESS. The control strategies can be classified into three general groups [62]: dynamic programming (DP), rule-based (RB) approaches, and methods based on the equivalent fuel consumption minimization (EFCM). Additionally, from the computational complexity and practical applicability perspective, they can be grouped in off-line and on-line approaches. DP is a widely used global optimization method for off-line controller optimization in DMU vehicles. Assuming an ideal case, i.e. perfect information on the future duty cycle, DP is used in obtaining fuel-optimal (combined) driving and energy management strategy in [44]. Using a simplified version of the EMR model from [49], a DP-based optimization of EMS for a regional train hybridized with Li-ion battery is proposed in [63]. The comparative assessment for three different degrees of hybridization (battery size) and two realistic mission profiles for a regional railway route indicated potential fuel savings reaching a significant level up to 18%. Control strategies based on DP typically serve as a benchmark for evaluating other (real-time) algorithms. Such an algorithm based on a sensitivity analysis and bisection method for a DMU equipped with a Li-ion battery is presented in [43], showing promising benefits in performance and especially computational cost compared to the DP method. The same algorithm is used in [45], with the analysis extended to DLC as alternative ESS technology. DP is also used as a benchmark in finding optimal dispatch (power distribution between ICEs) strategies [64,65], with fuel savings up to 7% compared to typical operation. In RB algorithms, event-triggered Boolean rules are derived from, for instance, heuristics or fuzzy rules based on experts' knowledge [46]. Due to their easy implementation and low computational times, these algorithms have been widely used in on-line ESS control applications [57,66]. However, unlike DP-based control, they cannot guarantee optimality. EFCM method is based on the conversion of electrical power into equivalent fuel consumption. Compared to RB approaches, it offers an explicit formulation of the optimization problem to minimize the instantaneous equivalent fuel consumption using equivalence factors. It is mostly combined with the optimization approaches such as DP and predictive control in defining causal controllers, where the supporting optimization techniques are used for defining the control reference values. EFCM as an on-line causal control is implemented in Siemens LMS Imagine.Lab Amesim simulation software used for the performance assessment of

hybrid DMUs with DE and DHM propulsion system, hybridized with Li-ion battery, DLC, or flywheel as ESS in [42].

Although the scientific literature on DMUs hybridization provides established models and comprehensive analyses of different hybrid system configurations and operational conditions, literature regarding the optimal sizing of ESS is rather scarce. The literature focuses primarily on the optimal control of the ESS with its size and configuration given beforehand or roughly estimated based on some main criteria, such as maximization of expected recuperated energy or electrification of auxiliaries, while neglecting the influence of the control strategy in place on the optimal size of the ESS. Studies in the automotive industry summarized in a recent review [52] have shown that by integrating these optimization levels, fuel-consumption benefits are obtained, which go beyond the results achieved with solely optimal control for a given topology. Additionally, practical and/or detailed implementations on real-life cases will face additional challenges reflected in consideration of numerous operational constraints and requirements, as well as in detailed data availability.

1.2. Paper contribution

In this paper, we propose a method to support the conversion decision of standard DMU vehicles to their hybrid counterpart by incorporating an optimally sized Li-ion battery-based ESS, while taking into account the trade-off between lower fuel consumption and hybridization cost. Using a detailed DMU powertrain simulation model, we then conduct the comparative assessment of fuel consumption and produced emissions of conventional and hybrid DMU vehicles. The presented research is part of a bigger project realized in collaboration with Arriva, the largest regional RU in the Netherlands. The results of this research will be used by the RU in the planning of future rolling stock and operations.

Based on the knowledge gaps presented in Section 1.1, the following are defined as the contribution of this paper:

1) A bi-level multi-objective optimization approach for determining the optimal size for the battery-based ESS by integrating the ESS sizing and control optimization levels, while at the same time incorporating emission-free and noise-free operation in stations in the problem formulation.
2) Two different power flow controls: (i) a non-causal optimal control based on dynamic programming that yields the absolute largest potential in fuel consumption reduction and global optimum for the primary optimization problem, and (ii) a causal sub-optimal rule-based control for emission-free and noise-free operation in stations and prolonged battery life by preventing frequent switches in charging/discharging cycles.
3) Application of the proposed method in a case study of two-coach DMU vehicles operating on a regional non-electrified railway network in the Netherlands, demonstrating potential benefits in terms of fuel savings and hybridization costs.

The paper is organized as follows. Section 2 presents the modeling of a hybrid DMU vehicle. The mathematical formulation of a bi-level optimization problem is given in Section 3. The application of the proposed methodology on a Dutch case study is provided in Section 4, followed by the discussion in Section 5. Section 6 concludes this paper with final remarks and future research directions.

2. Modeling of standard and hybrid DMU

The powertrain of standard diesel-electric multiple units consists of an internal combustion engine (ICE) directly connected to an AC electric generator (G), which is further connected via the rectifier and inverter to an AC electric motor (EM) located on the driveshaft. In the case of braking, the EM acts as the generator. The ICE supplies the mechanical

auxiliaries (e.g., hydraulic pump), while the electrical auxiliaries are connected to the existing DC link via a DC/AC inverter. The braking energy is, in this case, dissipated through the resistor, which is connected to the DC link via a DC/DC converter. Hybridization of diesel-electric DMU can be achieved by adding the appropriate ESS on the DC link, as shown in Fig. 1.

Compared to road transport, or even to railway freight transport, railway passenger transport is characterized by fixed routes with pre-determined stops and timetables, which also enable forecasts of typical driving behavior, speed profiles and duty cycles. Since the main aim of this paper is the analysis of the powertrain dynamics under typical operation conditions, rather than to assess the impact of different driving styles and traffic conditions, a backward quasi-static simulation approach [45,67] is adopted, following the system architecture shown in Fig. 1. The simulation model is developed with the MATLAB®/ Simulink© tool and OPEUS Simulink library [68]. In Fig. 2, the simulation structure following the system architecture from Fig. 1 is depicted, where the individual blocks represent the components of the model for the hybrid system. Corresponding to the backward simulation approach, the inputs of the simulation model are the DMU vehicle velocity and track geometry profiles, and the outputs are total fuel consumption with related emissions and ESS state-of-charge (SoC). The arrows indicate the numerical evaluation order of the model components, opposed to the direction of the physical power flow.

The following sub-sections provide the description of the components of the simulation model in Fig. 2, following the order of their numerical evaluation. For simplicity, the converters are assumed to have high constant efficiency; thus, their dynamics are not captured with this model. It is also assumed that electrical auxiliaries are characterized by a constant power demand $P_{elaux}[W]$. According to the control strategy implemented in the control unit, the total requested power for tracking the duty cycle is distributed between the ICE and the ESS (see Sections 3.2 and 4.3.3). A rheostat is used for converting the excess braking energy into heat, and it is used to keep the balance of energy in the model.

2.1. Vehicle

For the longitudinal vehicle dynamics, the tractive or braking effort at the wheel $F_w[N]$ can be expressed as

$$F_w(v(t)) = m_v \cdot a(t) + R_v(v(t)) + R_g(\gamma(s(t))) + R_c(\phi(s(t))) + R_t(l_t(s(t)), v(t))$$

with

$$R_v(v(t)) = r_0 + r_1 \cdot v + r_2 \cdot v^2$$

$$R_g(\gamma(s(t))) = m_v \cdot g \cdot sin(\gamma)$$

$$R_c(\phi(s(t))) = \begin{cases} m_v \cdot 0.03 & \text{if } \phi < 272m \\ m_v \cdot \dfrac{6.5}{\phi - 55} & \text{if } 272m \leq \phi < 2000m \\ 0 & \text{if } \phi \geq 2000m, \end{cases}$$

$$R_t(l_t(s(t)), v(t)) = 5 \cdot \dfrac{l_t}{S_t/S_v - 1} \cdot (0.036 \cdot v)^2,$$

(1)

where $t[s]$ is the time; $v[m/s]$ is the vehicle velocity; $s[m]$ is the distance traveled pre-calculated as $s = \int_0^t v(\tau)d\tau$; $a[m/s^2]$ is the acceleration pre-calculated as the derivative of vehicle velocity to time, i.e., $a = dv/dt$; $m_v[kg]$ denotes the total mass of the vehicle which takes into account the rotary inertia of the powertrain and the passengers weight, i.e. $m_v = (1 + \lambda) \cdot m_{tare} + m_{pax}$, with λ denoting the dimensionless rotating mass factor, $m_{tare}[kg]$ the vehicle tare weight, and $m_{pax}[kg]$ the total weight of passengers; $R_v[N]$ represents the vehicle resistances during motion, including roll resistance and air resistance, modeled as a quadratic function of the vehicle velocity using the Davis equation [69,70], where
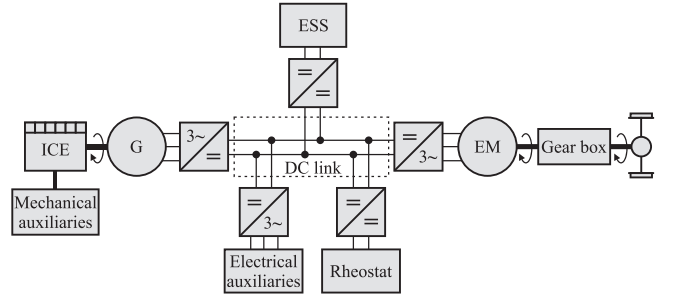

Fig. 1. Simplified schematic representation of hybrid system architecture for diesel-electric multiple unit.

non-negative coefficients $r_0[N]$, $r_1[N/(m/s)]$ and $r_2[N/(m/s)^2]$ are tuned based on the characteristics of the vehicle; $R_g[N]$ is the grade resistance, with $g = 9.81[m/s^2]$ representing the gravitational acceleration, and $\gamma[rad]$ the track gradient [71]; $R_c[N]$ denotes the curve resistance which depends on the radius of the curve $\phi[m]$, calculated using the approach of Hamburger Hochbahn AG [72] adopted by a number of European railways, and with these resistances set to zero for curves with radius higher than 2000 m; and $R_t[N]$ is the tunnel resistance which depends on the vehicle cross-sectional surface $S_v[m^2]$, tunnel length $l_t[m]$ and tunnel cross-sectional surface $S_t[m^2]$ [73,74], and with its value equal to zero for the tracks outside the tunnels.

Depending on the wheel diameter $d_w[m]$ and the train speed v, the torque at the wheel $T_w[Nm]$ and the rotational speed of the wheel $\omega_w[rad/s]$ can be calculated as [45]

$$T_w = F_w \cdot \frac{d_w}{2}$$

(2)

$$\omega_w = 2 \cdot \frac{v}{d_w}.$$

(3)

2.2. Axle gear

The axle gear transmits the power from the shaft to the wheels. With the constant gear ratio i_{ag}, the torque $T_{EM}[Nm]$ and the rotational speed $\omega_{EM}[rad/s]$ at the mechanical input of the axle gear can be computed by [45]

$$T_{EM} = \begin{cases} \dfrac{T_w}{i_{ag} \cdot \eta_{ag}} & \text{if } T_w \geq 0 \\ \dfrac{T_w \cdot \eta_{ag}}{i_{ag}} & \text{if } T_w < 0 \end{cases}$$

(4)

$$\omega_{EM} = \omega_w \cdot i_{ag},$$

(5)

where η_{ag} represents the efficiency of the gearbox, assumed to be constant.

2.3. Electric motor

The electric motor drive (EM) represents an induction machine, used either as a traction motor to move the train or as electro-dynamic brakes (generator mode), enabling the recuperation of the braking energy. Depending on the direction of the power flow (motor or generator operation mode), the electric power of the electric motor $P_{EM}[W]$ can be computed by [45]

$$P_{EM} = \begin{cases} \dfrac{T_{EM} \cdot \omega_{EM}}{\eta_{EM}} & \text{if } T_{EM} \geq 0 \\ T_{EM} \cdot \omega_{EM} \cdot \eta_{EM} & \text{if } T_{EM} < 0, \end{cases}$$
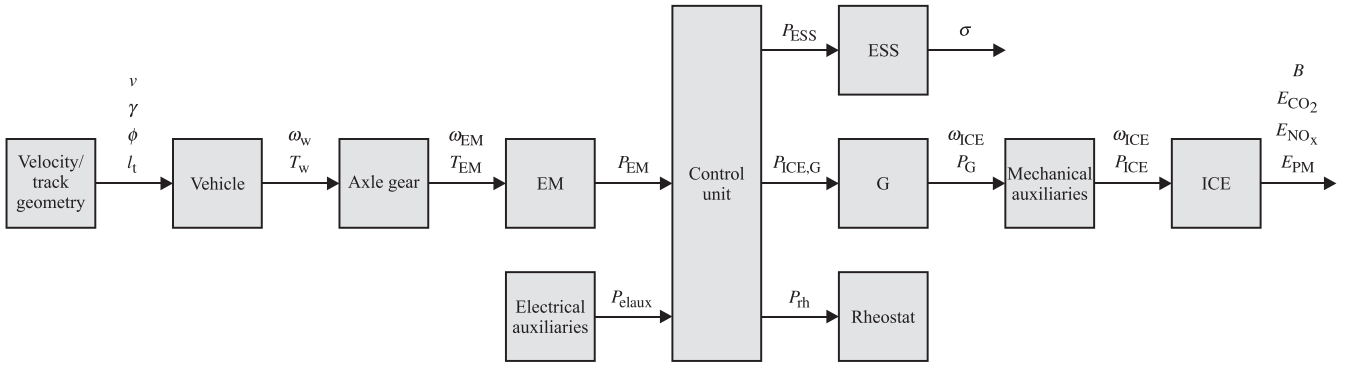
(6)

Fig. 2. Structure of the backward-looking simulation model for the hybrid diesel-electric multiple unit propulsion system.

where the efficiency $\eta_{EM} = f_{EM}(T_{EM}, \omega_{EM})$ is determined by a linear 2D-interpolation in the efficiency map of the EM.

2.4. Internal combustion engine – Electric generator set

The ICE, which is directly connected to the electric generator (G), is the primary traction source of the system architecture. The main output of the simulation model is the fuel consumption of the ICE, predicted by a measured static map. In the simulation model, the optimal ICE rotational speed ω_{ICE} [rad/s] is pre-calculated using the Nelder-Mead simplex method [75] for different possible levels of requested power and considering the generator's efficiency, mechanical auxiliaries power, and ICE specific fuel consumption. Physical separation of ICE-G set from the EM by a DC link enables the optimal working speed of the ICE for the requested power, irrespectively of the EM speed. With the given requested power $P_{ICE,G}$ [W], which represents the electrical output power of the generator, the mechanical input power of the generator P_G [W] is computed by

$$P_G = T_G \cdot \omega_{ICE} = \frac{P_{ICE,G}}{\eta_G}, \tag{7}$$

with the efficiency $\eta_G = f_G(T_G, \omega_G)$ determined by a linear 2D-interpolation in the efficiency map of the generator. Note that in the case of a standard DMU vehicle, the output power of the generator is equal to the total requested power for traction and powering electrical auxiliaries, i. e. $P_{ICE,G}(t) = P_{EM}(t) + P_{elaux}$, while in the case of a hybrid DMU it depends on the power split ratio between the two power sources, i.e. ICE-G set and ESS (see below). The mechanical auxiliaries power in this paper is assumed to be directly proportional to the ICE output power. With p_{maux} representing a constant ratio of the ICE output power used for the mechanical auxiliaries, the total demanded power from the ICE P_{ICE} [W] is calculated by

$$P_{ICE}(t) = \frac{P_G(t)}{(1 - p_{maux})}. \tag{8}$$

With the obtained simulation inputs, the angular velocity ω_{ICE}, and the requested ICE power P_{ICE}, the specific fuel consumption $\psi = f_f(P_{ICE}, \omega_{ICE})$ [kg/Ws] is computed using a 2D-interpolation of the static engine map. The total fuel consumption B [l], from time instant 0 to t, for the ICE becomes [45]:

$$B(t) = \int_0^t \frac{P_{ICE}(t) \cdot \psi(\tau)}{\rho} d\tau, \tag{9}$$

where ρ [kg/l] denotes the density of the fuel. In addition to the total fuel consumption, the produced emissions are included as additional performance indicators. The CO_2 emissions E_{CO2} [kg] depend on the amount and the type of fuel consumed and are calculated as [68]

$$E_{CO2}(t) = B(t) \cdot \varepsilon_{CO2}, \tag{10}$$

where ε_{CO2} [kg/l] represents the CO_2 emission factor for the fuel in use. The NO_x and PM emissions depend on the physical and operational characteristics of the engine (i.e., engine technology, angular velocity ω_{ICE}, and the requested power P_{ICE}). These are calculated similarly to the total fuel consumption by computing the emissions rate $\varepsilon_{NOx} = f_{NOx}(P_{ICE}, \omega_{ICE})$ [kg/s] and $\varepsilon_{PM} = f_{PM}(P_{ICE}, \omega_{ICE})$ [kg/s] using a 2D-interpolation of the static engine maps [68]

$$E_{NOx}(t) = \int_0^t \varepsilon_{NOx}(\tau) d\tau \tag{11}$$

$$E_{PM}(t) = \int_0^t \varepsilon_{PM}(\tau) d\tau. \tag{12}$$

2.5. Energy storage system

Lithium-ion battery is considered as the ESS in this paper. The simplified model of the battery is implemented for the equivalent electrical circuit shown in Fig. 3. It consists of a SoC-controled voltage source (open circuit voltage) U_{OC} [V] in series with a constant internal resistance R_{ESS} [Ω], which represents ohmic losses and depends on the direction of the ESS current I_{ESS} [A] (i.e., whether the battery is being charged or discharged). The ESS terminal voltage is denoted as U_{ESS} [V].

With a given ESS SoC $\sigma \in [0, 1]$, open circuit voltage U_{OC} and an internal resistance R_{ESS}, the current charging/discharging the ESS is governed by [76]

$$I_{ESS}(t) = \frac{U_{OC}(\sigma(t)) - \sqrt{U_{OC}(\sigma(t))^2 - 4 \cdot P_{ESS}(t) \cdot R_{ESS}(I_{ESS}(t))}}{2 \cdot R_{ESS}(I_{ESS}(t))}, \tag{13}$$

where P_{ESS} [W] represents the power profile at the ESS. Note that the open-circuit voltage U_{OC} depends on the ESS SoC, and that the internal
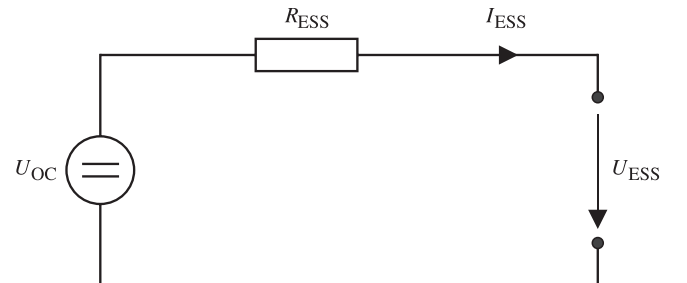

Fig. 3. Equivalent electrical circuit for the Li-ion battery-based energy storage system.

resistance depends on the direction of the power flow. With the ESS nominal capacity $C_{ESS,nom}$[As], the derivative of SoC to time is given by

$$\frac{d\sigma}{dt} = \frac{\sqrt{U_{OC}(\sigma(t))^2 - 4 \cdot P_{ESS}(t) \cdot R_{ESS}(I_{ESS}(t))} - U_{OC}(\sigma(t))}{2 \cdot R_{ESS}(I_{ESS}(t)) \cdot C_{ESS,nom}}. \tag{14}$$

Based on the ESS current, the terminal voltage U_{ESS} is given by:

$$U_{ESS}(t) = U_{OC}(\sigma(t)) - R_{ESS}(I_{ESS}(t)) \cdot I_{ESS}(t). \tag{15}$$

With the ESS parameters (open-circuit voltage, internal resistance and nominal capacity) provided at the battery cell level, for the battery consisting of n_{par} parallel branches with n_{ser} cells in series per branch their values at the ESS level can be determined by [45,67]

$$U_{OC} = n_{ser} \cdot U_{OC,cell} \tag{16}$$

$$R_{ESS} = \frac{n_{ser}}{n_{par}} \cdot R_{cell} \tag{17}$$

$$C_{ESS,nom} = n_{par} \cdot C_{cell,nom}, \tag{18}$$

where $U_{OC,cell}$, R_{cell}, and $C_{cell,nom}$ are the open-circuit voltage, internal resistance, and nominal capacity of one cell, respectively. The maximum charging/discharging power is limited by the maximum current while keeping the limits of the SoC $[\sigma_{min}, \sigma_{max}]$ as well as of the battery voltage $[U_{ESS,min}, U_{ESS,max}]$, with SoC and voltage assessed using (14) and (15), respectively. Additionally, to prevent overheating of the battery, the maximum charging and discharging power provided by the manufacturer have to be met. In this paper, the maximum continuous power $P_{ESS,cont}$ of the battery, which depends on the SoC and power direction (i.e., charging or discharging) is defined, thus not allowing short phases where power peaks exceed this threshold.

3. Optimal ESS sizing and control

This section presents an integrated ESS sizing end control, formalized as a bi-level multi-objective optimization problem. Using a nested co-ordination architecture, for each possible ESS size, an optimization of the energy management strategy (EMS) is done by dynamic programming. In this way, the lowest possible fuel consumption for the given ESS configuration (size) is guaranteed and the influence of the EMS choice on the primary optimization problem solution is removed.

3.1. Optimal **ESS sizing methodology**

With the battery-based ESS derived at the cell level, as described in Section 2, the size of the ESS can be represented with the variable $n_{ESS} = [n_{par} \; n_{ser}]$, where n_{par} denotes the number of battery parallel branches and n_{ser} the number of cells per branch. The weighted sum of fuel consumption and hybridization cost [77] is used in defining the objective function $J(n_{ESS})$ for the primary optimization problem:

$$J(n_{ESS}) = (1 - \alpha) \cdot \frac{J_1(\pi^*, n_{ESS})}{J_1^{nom}} + \alpha \cdot \frac{J_2(n_{ESS})}{J_2^{nom}}, \tag{19}$$

with $\alpha \in [0, 1]$ representing the assigned weight, $J_1(\pi^*, n_{ESS})$ is the lowest possible fuel consumption given the parameters n_{ESS} and the optimal control strategy π^* (see below), and $J_2(n_{ESS})$ is the total cost of hybridization. The nominal (largest possible) values J_1^{nom} and J_2^{nom} are used to normalize $J_1(\pi^*, n_{ESS})$ and $J_2(n_{ESS})$, respectively. Specific Li-ion battery cost of 200 EUR/kWh is assumed in this paper considering [78], thus resulting in the following hybridization cost function:

$$J_2(n_{ESS}) = 0.2 \cdot n_{par} \cdot n_{ser} \cdot C_{cell,nom} \cdot U_{cell,max}. \tag{20}$$

The objective is finding n_{ESS} that minimizes the objective function $J(n_{ESS})$ subject to a number of constraints that guarantee a required level of performance and satisfy the practical limitations. In this case,

inequality constraints are set based on the main hybridization requirements given in Section 1, and on an additional requirement of the sustenance of the battery SoC. SoC sustenance is achieved by including a constraint on the equality of battery SoC at the beginning and at the end of the duty cycle (see below). This constraint accounts for the vehicle circulation according to the periodic timetable, and at the same time, allows for a fair comparison with the conventional DMU. The resulting constraints are given as follows,

$$n_{par} \cdot n_{ser} \cdot P_{cell,cont,dch}(\sigma_{nom}) \geq P_{elaux} \tag{21}$$

$$n_{par} \cdot n_{ser} \cdot (E_{cell,max}(\sigma_{max}) - E_{cell,max}(\sigma_{nom})) \geq E_{elaux,stop,max} \tag{22}$$

$$n_{ser} \cdot U_{cell,min} \geq U_{ESS,min} \tag{23}$$

$$n_{ser} \cdot U_{cell,max} \leq U_{ESS,max} \tag{24}$$

$$n_{par} \cdot n_{ser} \cdot m_{cell} \leq m_{ESS,max}, \tag{25}$$

where $P_{cell,cont,dch}$ represents the maximum continuous discharging power of one cell, σ_{nom} is the nominal value for the battery SoC, $E_{cell,max}$ is the maximum energy of one cell, $E_{elaux,stop,max}$ is the maximum energy required for supplying electrical auxiliaries during stops, corresponding to the maximum dwell/turnaround time, $U_{cell,min}$ and $U_{cell,max}$ are the voltage limits of one cell, m_{cell} is the mass of one cell, and $m_{ESS,max}$ is the maximum allowed mass for the ESS. Constraints (21) and (22) ensure that the ESS can provide enough power and energy for supplying electrical auxiliaries during stops when the ICE is switched off. Constraints (23) and (24) are related to the ESS voltage limits conditioned by, for instance, DC link operating voltage, converter characteristics, etc. Finally, constraint (25) imposes the maximum allowed ESS mass, constrained by vehicle axle load limits, required traction performance, etc. The parameters $n_{ESS}^* = [n_{par}^* \; n_{ser}^*]$ represent the solution of the optimization problem, determined by minimizing the cost function:

$$n_{ESS}^* = \arg\left(\min_{n_{ESS}}\{J(n_{ESS})\}\right) \tag{26}$$

Deriving ESS at the cell level enables straightforward discretization of the search space, compared to the case of continuous decision variables where the choice of the discretization approach influences the quality of the solution. Due to a relatively low number of feasible solutions, the present approach also allows for the employment of an exhaustive (brute force) search algorithm instead of meta-heuristic approaches commonly used in case of continuous decision variables, thus guaranteeing to find a global optimum for the given optimization problem in a reasonable amount of time.

3.2. Optimal **energy management strategy**

The optimal energy management strategy aims at minimizing the total fuel consumption B (and related CO_2 emissions E_{CO2}) of the ICE by adjusting the power flows at the DC link, in particular by separating the total demanded power at the DC link between the ICE-G set and the ESS, while at the same time ensuring the sustenance of the ESS SoC, represented by

$$\sigma(T) = \sigma(0) = \sigma_{nom}, \tag{27}$$

where T[s] denotes the total duration of the trip and the final time instant. The total demanded power at the DC link P_{DC} represents the sum of the required traction power P_{EM} and electrical auxiliaries power P_{elaux}:

$$P_{DC}(t) = P_{EM}(t) + P_{elaux}. \tag{28}$$

In order to determine the optimal operating strategy, a control variable $x(t) \in [-1, 1]$ is introduced, representing the split of the total requested power $P_{DC}(t)$ between the ICE (via G) and the ESS. Based on

the instantaneous values of the control variable x, the total requested power P_{DC}, and the vehicle velocity v given as the main simulation input, the power flow from the ICE-G set and ESS is given by the following equations:

$$P_{ICE,G}(v, P_{DC}, x) = \begin{cases} (1-x) \cdot P_{max,1} + (P_{DC} - P_{max,1}) & \text{if } v > 0, P_{DC} > 0, x \in [0,1] \\ -x \cdot P_{max,2} + P_{DC} & \text{if } v > 0, P_{DC} > 0, x \in [-1,0) \\ 0 & \text{if } v = 0 \lor P_{DC} \le 0 \end{cases}$$

(29)

$$P_{ESS}(v, P_{DC}, x) = \begin{cases} x \cdot P_{max,1} & \text{if } v > 0, P_{DC} > 0, x \in [0,1] \\ x \cdot P_{max,2} & \text{if } v > 0, P_{DC} > 0, x \in [-1,0) \\ P_{max,3} & \text{if } v > 0, P_{DC} \le 0 \\ P_{DC} & \text{if } v = 0, \end{cases}$$

(30)

where $P_{max,1} = \min\{P_{DC}, P_{ESS,max,dch}\}$, $P_{max,2} = \min\{(P_{ICE,G,max} - P_{DC}), -P_{ESS,max,ch}\}$ and $P_{max,3} = \max\{P_{DC}, P_{ESS,max,ch}\}$, with $P_{ESS,max,dch}$ and $P_{ESS,max,ch}$ denoting the maximum ESS discharging and recuperation (charging) power, respectively. In the case of $x = 1$ and $P_{DC} \le P_{ESS,max,dch}$, the ESS provides the total requested power P_{DC} ("pure electrical mode"), while for $x = 0$ the total power demand P_{DC} is provided solely by ICE ("pure ICE mode"). The so-called "power boost mode," where the total requested power is provided by ICE and ESS together, represents the case of $0 < x < 1$ or the case of $x = 1$ and $P_{DC} > P_{ESS,max,dch}$. In "load level increase mode" with negative values of x, the ICE provides more than the requested power P_{DC}, where the excess power is used for recharging the ESS. Note that during stops ($v = 0$), the ICE is switched off and the ESS provides the total requested power, while in case of negative values of total requested power ($P_{DC} \le 0$), the ICE operates with no load at idling speed and the ESS is being recharged ("recuperation mode").

In order to obtain a fuel-optimal operating strategy, the DP approach according to Bellman [79] is used, following the methodology presented in [45] and [80], and with respect to the current system architecture and operation characteristics. First, the continuous optimization problem had to be converted into a multi-stage decision process through discretization, allowing for a numerical solution. Time, as an identifier of the optimization horizon, is discretized into $t \in \{t_k | k = 0, \cdots, K\}$ with K regular time intervals and discretization interval (step length) equal to $\Delta t = (t_K - t_0)/K = T/K$. The state variable is discretized into $\sigma \in \{\sigma_i | i = 1, \cdots, I\}$ for each discrete time with I equally distributed values for the ESS SoC over the interval $[\sigma_{min}, \sigma_{max}]$, and with $\sigma_1 = \sigma_{min}$ and $\sigma_I = \sigma_{max}$. In this way, the discretized state-time space is defined with a fixed grid, see Fig. 4.

The control variable $x(\sigma(t_k), t_k) \in X = \{x_j | j = 1, \cdots, M\}$, applied to each state in the given state-time space, is discretized into M equally distributed values for the power split ratio over the interval $[-1, 1]$, with $x_1 = -1$ and $x_M = 1$.

With given vehicle and ESS parameters, as well as precalculated velocity $v(t_k)$ and total demanded power $P_{DC}(t_k)$ for each time step t_k, the dynamics of the system are given by

$$\sigma(t_{k+1}) = f_\sigma(\sigma(t_k), x(\sigma(t_k), t_k); v(t_k), P_{DC}(t_k)), k = 1, \cdots, K-1,$$

(31)

with $\sigma(t_{k+1})$ representing the resulting state (ESS SoC) one step ahead of $\sigma(t_k)$, obtained by applying the control variable $x(\sigma(t_k), t_k)$ to the state $\sigma(t_k)$, where the transition function f_σ consists of a sequence of equations, i.e., (30) and (14), describing the given evolution from the initial to the resulting state.

Let $\pi = \{x(\sigma(t_k), t_k) | k = \{0, \cdots, K-1\}\}$ denote a control policy. Further, let the total cost-to-go $B_\pi(\sigma(t_0))$ of applying π with initial state $\sigma(t_0) = \sigma_{nom}$ be

$$B_\pi(\sigma(t_0)) = \sum_{k=0}^{K-1} f_k(\sigma(t_k), x(\sigma(t_k), t_k); v(t_k), P_{DC}(t_k)) + f_K(\sigma(t_K)),$$

(32)

with the transition cost function f_k defined as the fuel consumption during one step, when the control variable $x(\sigma(t_k), t_k)$ is applied to the
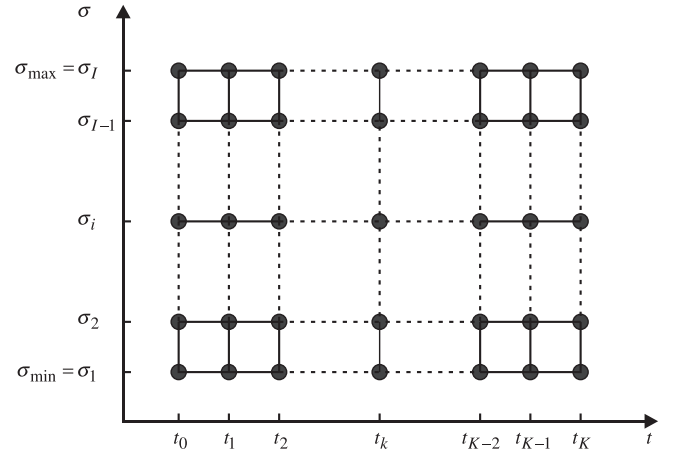

Fig. 4. Discretized state-time space for the application of dynamic programming algorithm.

state $\sigma(t_k)$, given by the sequence of equations (29), (7)–(9), and $f_K(\sigma(t_K))$ denoting the terminal cost for the resulting state $\sigma(t_K)$ in the last stage of the horizon, defined in the way that forces constrained final state (27), and given by

$$f_K(\sigma(t_K)) = \begin{cases} 0 & \text{if } \sigma(t_K) = \sigma(t_0) = \sigma_{nom} \\ Inf & \text{otherwise,} \end{cases}$$

(33)

where Inf is a big number representing the penalty. The objective is to find the optimal control policy π^* that minimizes the right-hand side of (32), i.e., that leads to the optimal total cost-to-go $B^*(\sigma(t_0))$

Based on the optimality principle [81], the DP algorithm evaluates the optimal cost-to-go function $B^*(\sigma(t_k))$ backwards in time at every node of the discretized state-time space $\sigma(t_k) \in \{\sigma_i | i = 1, \cdots, I\}$. With the remaining minimum costs starting from the state $\sigma(t_{k+1})$ up to the final stage t_K known, the optimization problem can be rewritten as the recursion from $k = K-1$ down to $k = 0$,

$$B^*(\sigma(t_k)) = \min_{x(\sigma(t_k), t_k) \in X} \{f_k(\sigma(t_k), x(\sigma(t_k), t_k); v(t_k), P_{DC}(t_k)) + B^*(\sigma(t_{k+1}))\},$$

(34)

where $\sigma(t_{k+1})$ is calculated using (31). If the resulting state $\sigma(t_{k+1})$ is not equal to one of the I discrete values of the state σ_i, the remaining minimum costs $B^*(\sigma(t_{k+1}))$ are determined by an interpolation between the two closest states.

By backward iteration in time and using (34), the optimal control given by an argument that minimizes the right-hand side of (34) for all the states in the horizon can be found, with the output of the algorithm given in the form of an optimal control map. With the given optimal control map, by forward simulation starting from the initial state $\sigma(t_0) = \sigma_{nom}$ and using (31), the optimal control sequence and the optimal state trajectory for the entire horizon can be derived. Since the optimal control in the map is only given for the discrete points in the state-time space, it is therefore interpolated when the actual resulting state does not coincide with the discrete points in the state space [80]. Note that since all the states in the last time step t_K except one state (i.e., $\sigma(t_K) = \sigma_{nom}$) have an extremely high cost (i.e., Inf), any control sequence which leads to any other final state, results in a high total fuel consumption and is neglected [82]. The resulting optimal ESS control is characterized by frequent switches in the power split ratio [45]. This characteristic of a DP-based control, together with the required computation time, hinders its on-line applicability. However, the obtained results can be regarded as the global optimum. The obtained minimum total cost $B^*(\sigma(t_0))$ represents the lowest possible fuel consumption $J_1(\pi^*, n_{ESS})$ related to the given ESS size, further implemented in (19).
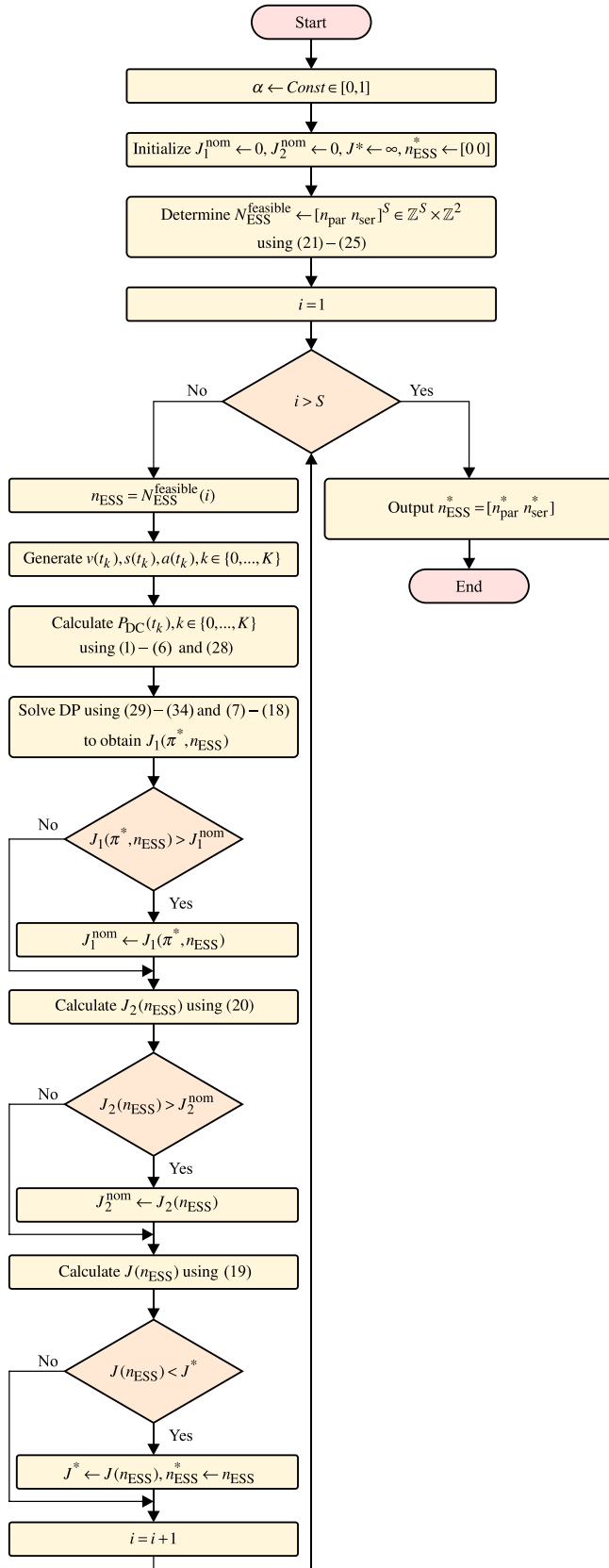
Start

$\alpha \leftarrow Const \in [0,1]$

Initialize $J_1^{\text{nom}} \leftarrow 0, J_2^{\text{nom}} \leftarrow 0, J^* \leftarrow \infty, n_{\text{ESS}}^* \leftarrow [0\ 0]$

Determine $N_{\text{ESS}}^{\text{feasible}} \leftarrow [n_{\text{par}}\ n_{\text{ser}}]^S \in \mathbb{Z}^S \times \mathbb{Z}^2$
using $(21)-(25)$

$i = 1$

$i > S$ — No / Yes

Yes → Output $n_{\text{ESS}}^* = [n_{\text{par}}^*\ n_{\text{ser}}^*]$ → End

No →

$n_{\text{ESS}} = N_{\text{ESS}}^{\text{feasible}}(i)$

Generate $v(t_k), s(t_k), a(t_k), k \in \{0,...,K\}$

Calculate $P_{\text{DC}}(t_k), k \in \{0,...,K\}$
using $(1)-(6)$ and (28)

Solve DP using $(29)-(34)$ and $(7)-(18)$
to obtain $J_1(\pi^*, n_{\text{ESS}})$

$J_1(\pi^*, n_{\text{ESS}}) > J_1^{\text{nom}}$ — No / Yes

Yes → $J_1^{\text{nom}} \leftarrow J_1(\pi^*, n_{\text{ESS}})$

Calculate $J_2(n_{\text{ESS}})$ using (20)

$J_2(n_{\text{ESS}}) > J_2^{\text{nom}}$ — No / Yes

Yes → $J_2^{\text{nom}} \leftarrow J_2(n_{\text{ESS}})$

Calculate $J(n_{\text{ESS}})$ using (19)

$J(n_{\text{ESS}}) < J^*$ — No / Yes

Yes → $J^* \leftarrow J(n_{\text{ESS}}), n_{\text{ESS}}^* \leftarrow n_{\text{ESS}}$

$i = i + 1$

Fig. 5. Flowchart for the proposed bi-level optimization algorithm based on nested architecture.

3.3. Bi-level optimization methodology

The optimization problem is solved using the following methodology. First, the feasible discrete search space is determined based on the constraints (21)–(25) that guarantee the required level of performance and satisfy technical and physical limitations. The feasible search space is given by a vector of pairs representing feasible battery configurations in terms of number of parallel branches and number of cells per branch, i.e. by $N_{\text{ESS}}^{\text{fesible}} = \left[n_{\text{par}}\ n_{\text{ser}} \right]^S$, with S denoting the number of feasible battery configurations. Using the exhaustive (brute force) search, for each point in the feasible search grid (ESS configuration), the fuel-optimized speed trajectory that comply with the given timetable and track and vehicle parameters (including the maximum tractive effort (see Fig. 8), and the additional mass of the ESS which influences acceleration/braking characteristics) is generated using the algorithm described in [83]. The algorithm is based on optimizing switching points between cruising and coasting using a bisection method. In this way, the influence of different driving styles on the results is eliminated. Based on the generated speed trajectory, the power profile at the DC link representing the total requested power is computed by evaluating simulation blocks located on the left side of the control unit in the simulation model in Fig. 2. The optimal control strategy is then determined using DP, and the fuel consumption and hybridization costs are evaluated. This sequence is repeated until all feasible solutions are evaluated. The optimal size of the ESS is then determined by solving the problem in (26). The algorithm for the presented bi-level optimization problem based on the nested architecture is illustrated in Fig. 5.

4. Case study of regional railway services in the Northern Netherlands

The methodology proposed in the previous section is applied to a case study of DMUs from the RU Arriva, operating on the Dutch regional railway network. In the following sub-sections, the input parameters are first defined for the selected railway line and the DMU vehicle, followed by an analysis of different scenarios.

4.1. Track parameters

We analyze the railway passenger services provided on the non-electrified regional lines in the Northern part of the Netherlands, in the provinces of Friesland and Groningen. For this study, we selected the train services provided on the 54 km long main railway line, which connects the cities Leeuwarden and Groningen. Two different types of services are being provided by the RU on this line – stopping and express, with the corresponding stops shown in Fig. 6a. In this study, optimal ESS size and energy management strategy are determined for the vehicles employed on the stopping services with seven intermediate stops.

Due to the difference in line resistances as well as maximum speed limits for the two opposite directions, the vehicle round trip is analyzed, which is based on the current periodic timetable and vehicle circulation plan for the given railway line. In order to include relevant factors affecting the vehicle dynamics, track geometry parameters were extracted. Fig. 6b shows the track height profile compared to the Normal Amsterdam Level (in Dutch, *Normaal Amsterdams Peil, NAP*), and Fig. 6c the location of the curves with a radius lower than 2000 m. There are no tunnels on this part of the network. The maximum allowed speed in both directions is shown in Fig. 6d. Table 1 shows an example of the vehicle round trip with given departure times from each stop. Dwell time of 30 s is assumed at intermediate stops. According to the timetable, layover times at the terminal stops are 11 min in Leeuwarden and 12 min in Groningen.
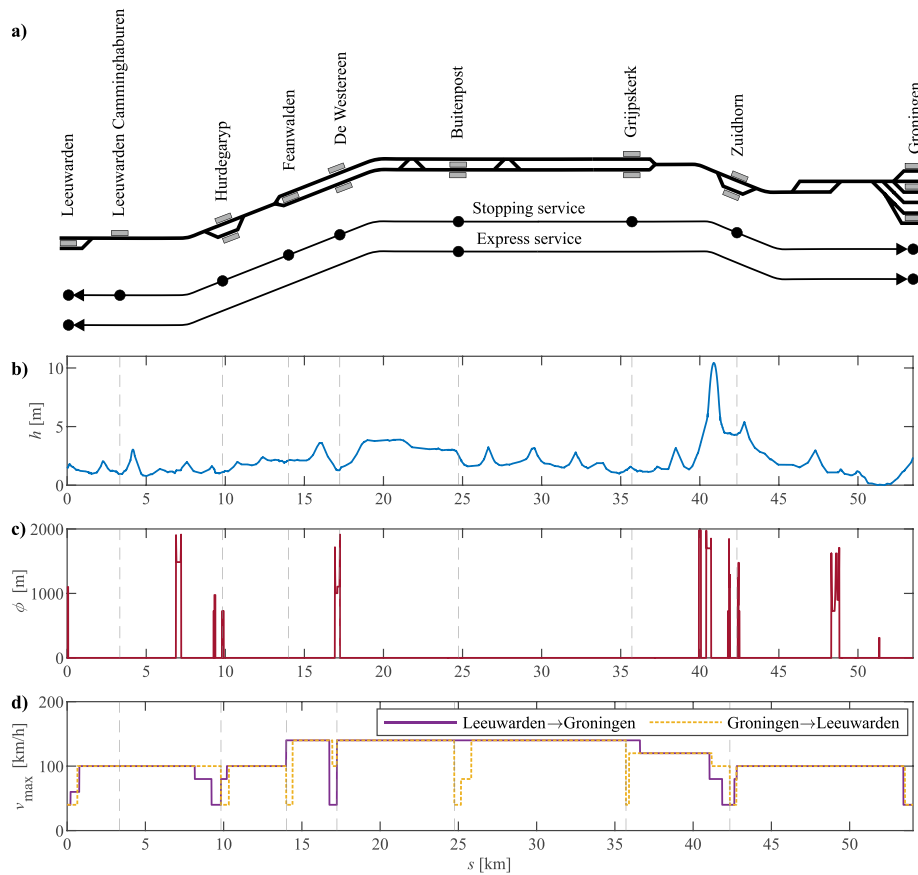
Fig. 6. Railway line Leeuwarden – Groningen: (a) schematic representation with indicated stops for stopping and express services, (b) track height compared to Normal Amsterdam Level, (c) curves with radius lower than 2000 m, and (d) maximum allowed speed for the two opposite directions.

Fig. 7. Graphical representation of Stadler GTW 2/6 diesel-electric multiple unit [84].

4.2. Vehicle *parameters*

The RU Arriva currently provides the services on the network with a fleet of 22 two-coach GTW 2/6 and 29 three-coach GTW 2/8 DMUs from the Swiss manufacturer Stadler. The GTW 2/6 DMU (Fig. 7) has been selected for the analysis in this paper. The vehicle parameters provided by the RU are shown in Table 2.

Since the additional mass of ESS affects both vehicle acceleration and braking performance, it is essential that the velocity profile, which is the main simulation input, complies with the maximum available traction force. The maximum tractive effort curve for GTW 2/6 DMUs is shown in Fig. 8a, where the negative values are assumed for braking. It consists of a constant maximum tractive effort part for the vehicle velocities $v \leq 27$ km/h, and a constant maximum power hyperbola for $v \geq 27$ km/h. Note that in the case of a conventional DMU, braking power is dissipated at the resistors.

Due to the unavailability of detailed characteristics for GTW's powertrain components (EM, G, and ICE), available sources that provide the data on the powertrain components with similar maximum power/torque are used. The European project CleanER-D [86] reported specifications for the powertrain components in different railway vehicles. Available data include detailed and validated efficiency, fuel
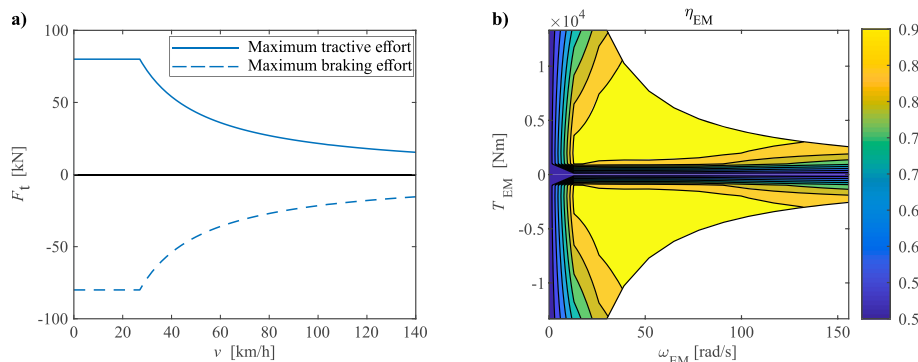

Fig. 8. (a) Tractive effort vs. speed diagram, and (b) reconstructed electric motor efficiency map for Stadler GTW 2/6 diesel-electric multiple unit.

Table 1

Departure times for the vehicle round trip on the line Leeuwarden-Groningen.

Stop	Departure time (hh:mm)	
	From Leeuwarden to Groningen	From Groningen to Leeuwarden
Leeuwarden	hh : 51	hh + 2 : 40 (arrival)
Leeuwarden C.	hh : 54	hh + 2 : 35
Hurdegaryp	hh + 1 : 01	hh + 2 : 30
Feanwalden	hh + 1 : 05	hh + 2 : 25
De Westereen	hh + 1 : 08	hh + 2 : 20
Buitenpost	hh + 1 : 16	hh + 2 : 15
Grijskerk	hh + 1 : 23	hh + 2 : 06
Zuidhorn	hh + 1 : 30	hh + 2 : 01
Groningen	hh + 1 : 39 (arrival)	hh + 1 : 51

Table 2

Main input parameters for Stadler GTW 2/6 diesel-electric multiple unit.

Parameter	Value	Unit	Description
m_{tare}	70.4	t	Empty mass[a]
λ	0.05	–	Rotating mass factor[b]
m_v	77	t	Total mass including passengers[b]
r_0	1001	N	Davis equation coefficient (constant term)[b]
r_1	22.3	N/(km/h)	Davis equation coefficient (linear term)[b]
r_2	0.1	N/(km/h)^2	Davis equation coefficient (quadratic term)[b]
v_{max}	140	km/h	Maximum velocity[c]
a_{max}	1.05	m/s^2	Maximum acceleration[b]
a_{min}	−1	m/s^2	Maximum deceleration[b]
$P_{ICE,max}$	2×390	kW	Diesel engine maximum power[a]
$P_{EM,max}$	2×400	kW	Electrical motor maximum power[a]
d_w	0.86	m	Wheel diameter[c]
i_{ag}	1.7218	–	Constant axle gear ratio[d]
η_{ag}	97	%	Gear box efficiency[e]

Source: [a]Giro Batalla & Feenstra [84]; [b]Provided by Arriva; [c]Stadler Bussnang AG [85]; [d]Determined from the ratio between the maximum rotational speed of the electrical motor $\omega_{EM,max} = 1487$rpm given in [84] and the maximum rotational speed of the wheel corresponding to the maximum vehicle speed $v_{max} = 140$km/h, as $i_{ag} = \omega_{EM,max}/\omega_{w,max}$; [e]Adopted from Prohl [68].

consumption and emissions maps. Thus, this source is used in deriving and reconstructing parameters for the DMU analyzed in this paper. The efficiency map of GTW's EM with maximum power $P_{EM,max} = 400$kW is derived using the normalized efficiency map $\eta_{EM} = f_{EM}^{norm}(\omega_{EM}/\omega_{EM,max}, T_{EM}/T_{EM,max})$ provided in [87]. The resulting efficiency map as a function of torque and angular speed is given in Fig. 8b.

In order to derive the input parameters for the GTW's ICE-G set, data provided in the same source [87] are used, wherein the maximum power/torque characteristics, generator's normalized efficiency map $\eta_G = f_G^{norm}(\omega_G/\omega_{G,max}, T_G/T_{G,max})$, ICE specific fuel consumption map $\psi = f_\psi(\omega_{ICE}, P_{ICE})$, as well as NO$_x$ and PM emissions rate maps $\varepsilon_{NOx,PM} = f_{NOx,PM}(\omega_{ICE}, P_{ICE})$ are given for various ICE sizes (with a maximum power of 360, 560 and 1000 kW). The available 360 kW ICE is very similar to the one found in GTW DMU, as both represent adaptations of a heavy-duty truck ICE, complying with Stage IIIA standard. As the maximum power of the ICE found in GTW DMU (390 kW) differs from the ICEs found in the given source, the ICE static maps had to be reconstructed. For this, a scaling methodology based on so-called Willans lines is employed [88–90]. A second-order polynomial approximates the engine specific fuel consumption for each ICE operating speed, while the ICE torque is scaled linearly with a scaling factor S_{ICE}. The approximation of specific fuel consumption can be written as

$$\psi(\omega_{ICE}, T_{ICE}) = C_0(\omega_{ICE}) \cdot S_{ICE} + C_1(\omega_{ICE}) \cdot T_{ICE} + C_2(\omega_{ICE}) \cdot \frac{T_{ICE}^2}{S_{ICE}}. \quad (35)$$

The scaling factor represents the ratio between scaled engine maximum power $P_{ICE,max}$ and the original ICE maximum power $P_{ICE,max0}$. The accuracy of this approach increases as the size of the approximated ICE is closer to the size of the original ICE [78]; thus, the ICE with a maximum power of 360 kW is chosen, resulting in the scaling factor

$$S_{ICE} = \frac{P_{ICE,max}}{P_{ICE,max0}} = 1.0833. \quad (36)$$

The second-order polynomial approximation coefficients C_0, C_1 and C_2 are first calculated by numerically solving a system of equations for each T_{ICE} vs. ω_{ICE} data point from the original ICE specific fuel consumption map using the least-squares method while setting the scaling factor $S_{ICE} = 1$ in (35). Then, by inserting the obtained polynomial coefficients (Fig. 9a) into (35), and by scaling the torque with the scaling factor S_{ICE} given in (36), the ICE specific fuel consumption for GTW DMU is reconstructed (Fig. 9b). The efficiency map for G is obtained in the same way as for EM, while the torque is scaled with the scaling factor S_{ICE}.

Fuel density $\rho = 825$g/l and CO$_2$ emission factor $\varepsilon_{CO2} = 3.175$kg/l for diesel fuel is adopted from [68]. The Willans line technique is also applied in reconstructing the ICE NO$_x$ and PM emissions rate maps for GTW DMU, shown in Fig. 9c and d. In this paper, NO$_x$ and PM emissions are included in the analysis as the additional indicators to the primary indicator of total fuel consumption. However, with the available emission rate maps, they can easily be included in the optimization problem as additional terms of the objective functions (19), which is left for future research.

The Saft Ion-OnBoard® Regen Li-ion commercial battery based on sLFP (Super Lithium Iron Phosphate) chemistry [91] is considered to define the parameters for the ESS sizing and energy management problem. The parameters are extracted at the cell level by scaling down the values provided for this particular battery in [92] with respect to the number of its cells. The resulting values are given in Table 3, and the resulting cell open-circuit voltage as a function of SoC is shown in Fig. 10. In order to account for battery aging effects, end-of-life (EoL) values for nominal cell capacity, maximum energy and internal resistance are adopted.

4.3. Results

All numerical simulations/calculations are performed in MATLAB®/Simulink© environment, on a PC with Intel® Core™ i7-8650U 1.9 GHz CPU and 8 GB of RAM. A fixed time step $\Delta t = 1$s is adopted in all experiments, with the ode3 (Bogacki-Shampine) solver used for numerical integration. The results in terms of resulting fuel consumption and related emissions are compared with the conventional DMU without an ESS. Estimation of the fuel consumption and related emissions of conventional DMU is done by evaluating the model in Fig. 2, with the total requested power provided by ICE.

4.3.1. Optimal ESS size and resulting fuel consumption and emissions

In order to determine optimal ESS size for the hybridized DMU, the feasible search space representing possible ESS configurations is determined first, such that it satisfies the limitations on requested power from electrical auxiliaries $P_{elaux} = 45$kW, maximum required energy from ESS for supplying the auxiliaries in terminal stops $E_{elaux,stop,max} = 9$kWh, corresponding to the layover time of 12 min in Groningen, ESS voltage limits $U_{ESS,min} = 500$V and $U_{ESS,max} = 1000$V, and maximum allowed mass for ESS $m_{ESS,max} = 2.5$t. Fig. 11 shows the resulting feasible region of the discrete search space for the ESS sizing problem, bounded by the five inequality constraints (21)–(25), which contains 228 possible ESS configurations (orange dots in the grid). Lower and upper boundary lines for the number of cells per branch (n_{ser}), reflect the constraints on the ESS voltage. The lower boundary line for the total number of cells, i. e. $n_{ESS} = n_{par} \cdot n_{ser}$, is derived from the constraint on the required energy
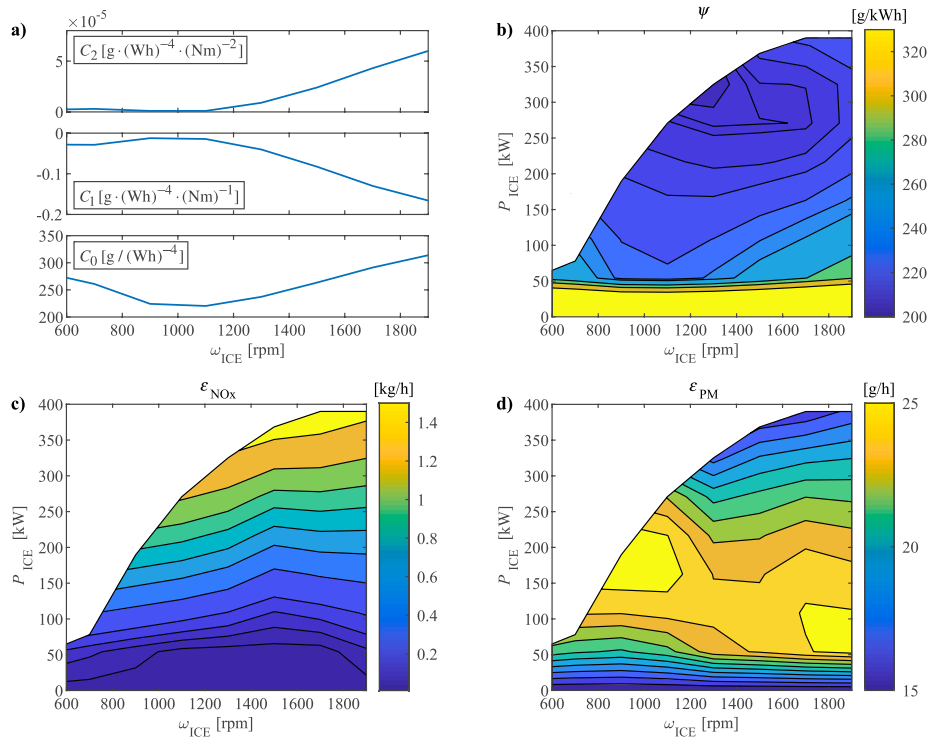
Fig. 9. (a) Rotational speed-dependent coefficients of the polynomial approximation of specific fuel consumption, (b) specific fuel consumption map, (c) NOₓ emissions rate map, and (d) PM emissions rate map of GTW 2/6 internal combustion engine.

Table 3
Li-ion battery cell parameters.

Parameter	Value	Unit	Description
σ_{max}	90	%	Maximum SoC
σ_{nom}	50	%	Nominal SoC
σ_{min}	10	%	Minimum SoC
$U_{cell,max}$	3.8	V	Maximum cell voltage
$U_{cell,min}$	2.5	V	Minimum cell voltage
$R_{cell,ch}$	0.002700	Ω	Internal cell resistance during charging
$R_{cell,dch}$	0.002716	Ω	Internal cell resistance during discharging
$C_{cell,nom}$	16.8	Ah	Cell nominal capacity
$P_{cell,cont,dch}(\sigma_{max})$	0.626310	kW	Cell maximum continuous discharging power at maximum SoC
$P_{cell,cont,dch}(\sigma_{nom})$	0.569312	kW	Cell maximum continuous discharging power at nominal SoC
$P_{cell,cont,dch}(\sigma_{min})$	0.490697	kW	Cell maximum continuous discharging power at minimum SoC
$P_{cell,cont,ch}(\sigma_{max})$	−0.384697	kW	Cell maximum continuous charging power at maximum SoC
$P_{cell,cont,ch}(\sigma_{nom})$	−0.534478	kW	Cell maximum continuous charging power at nominal SoC
$P_{cell,cont,ch}(\sigma_{min})$	−0.599807	kW	Cell maximum continuous charging power at minimum SoC
$E_{cell,max}(\sigma_{max})$	0.050974	kWh	Cell maximum energy at maximum SoC
$E_{cell,max}(\sigma_{nom})$	0.027133	kWh	Cell maximum energy at nominal SoC
$E_{cell,max}(\sigma_{min})$	0.005254	kWh	Cell maximum energy at minimum SoC
m_{cell}	2.122500	kg	Cell mass

Fig. 10. The open-circuit voltage of one Li-ion battery cell as a function of state-of-charge.

ESS should be able to provide during stops, while the maximum number of cells is limited by the maximum allowed mass for the ESS. The constraint reflecting the minimum required ESS power is, in this case, already fulfilled with the energy-related requirement and does not restrict the search space.

For the application of the DP algorithm, the optimal control problem is discretized into $K = 7200$ regular time steps, with the corresponding time step length equal to 1 s, $I = 401$ values for the SoC σ_i,
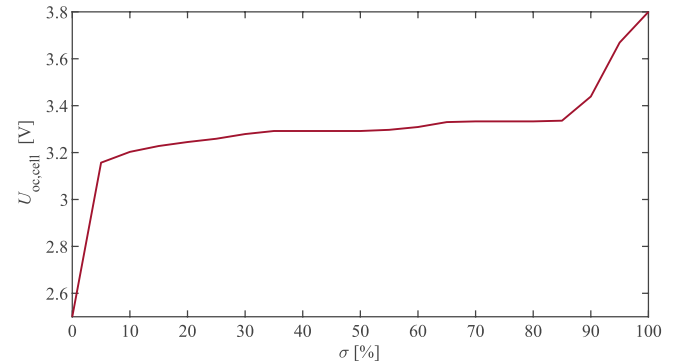
$i \in \{1, \cdots, 401\}$, equally distributed over the interval $[0.1, 0.9]$, and $M = 201$ values for the power split ratio $x_j, j \in \{1, \cdots, 201\}$, equally distributed over the interval $[-1, 1]$. The ESS SoC at the beginning and the end of the round trip is set to $\sigma_{nom} = 0.5$. The computationally efficient generic DP function [93] is used in determining optimal ESS control, providing a significant reduction of computation time and numerical errors. Optimal control and corresponding fuel consumption were obtained in about 3 min on average per feasible ESS configuration. The weight α in (19) is set to 0.2 to reflect a moderate preference towards lower fuel consumption over total hybridization cost. Following the methodology given in Section 3, the obtained optimal ESS consists of $n^*_{par} = 2$ parallel branches with $n^*_{ser} = 231$ cells in series per branch. The corresponding hybridization costs are 5898.82 EUR. Fig. 12 shows the simulation results for the hybrid DMU with optimally sized ESS, including the vehicle velocity profile, power split between the ICE and ESS, and the ESS SoC during the trip. As shown, the ESS provides the total requested power during stops with the ICE switched off, thus satisfying the primary hybridization requirement (emissions-free and
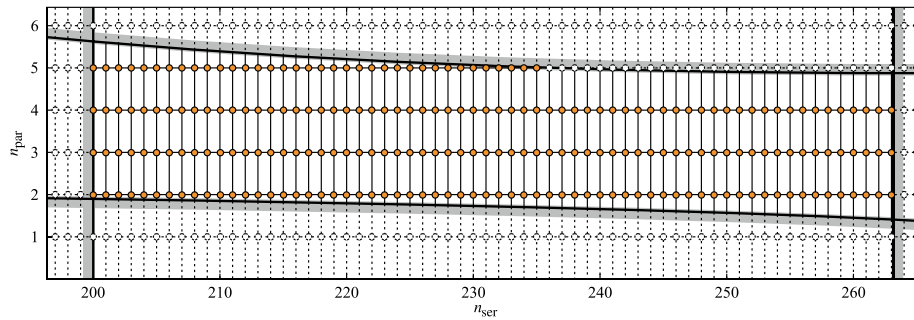
Fig. 11. The feasible region of the discrete search space for optimal energy storage system sizing problem.

noise-free operations during stops). At the same time, the request for SoC sustenance is achieved, despite the significant ESS discharge in terminal railway stations.

The resulting fuel consumption and related emissions for both conventional and hybrid DMU are given in Table 4. Compared to the conventional DMU vehicle, its hybridized counterpart with optimally sized and controlled ESS offers fuel savings and CO_2 emissions reduction of 29.9%. For the additional indicators representing local pollutant emissions, the simulation results show a 6.1% reduction in NO_x emissions and a 22.4% reduction in PM emissions.

4.3.2. Trade-off between lower fuel consumption and hybridization cost

In order to further investigate the influence of the weight α on the trade-off between better fuel economy and lower hybridization cost, additional analysis was conducted by changing the weight value between 0 and 1, representing the most fuel and cost-efficient solutions, respectively. The results of the analysis are given in Fig. 13 and Table 5. The results indicate that the increase in fuel consumption across α (i.e., between fuel consumption for $\alpha = 0$ and $\alpha = 1$) is 7.5%, giving the fuel savings compared to the conventional DMU vehicle (Table 4) ranging from 34.5% down to 29.6%. The total cost of hybridization is, at the

Table 4
Fuel consumption and produced emissions for conventional and hybrid diesel-electric multiple unit with optimally sized energy storage system.

Indicator	Unit	Conventional DMU	Hybrid DMU	Savings (%)
B	liter	116.7103	81.8187	29.9
E_{CO2}	kg	370.5552	259.7744	29.9
E_{NO_x}	kg	1.4972	1.4059	6.1
E_{PM}	kg	0.0858	0.0666	22.4

same time, reduced by 54.6%.

Compared with the previous case ($\alpha = 0.2$) further reduction of fuel consumption of about 5% would require a significant increase in total hybridization cost of more than 30%. However, by considering the cumulative fuel savings and the vehicle life cycle duration, the investment return period would be relatively short. Results also indicate that the proposed optimization approach excluded the possibility of oversizing the ESS, as would be the case of the only criterion for hybridization being the maximum possible ESS size, conditioned with the mass limitation. In this way, further increase for 25% of total hybridization cost without any improvement of fuel economy is prevented.
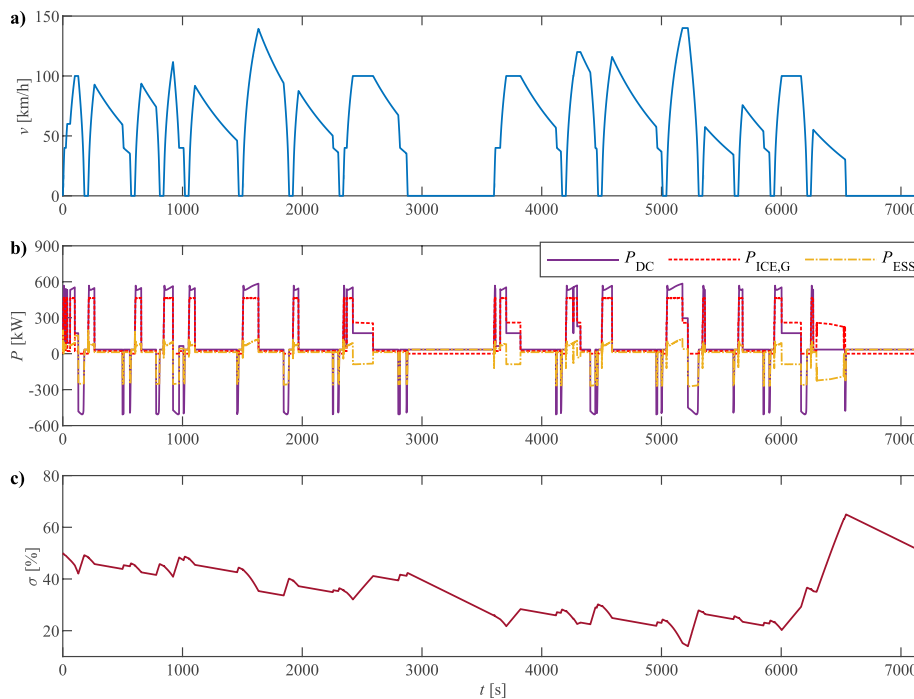

Fig. 12. Simulation results for hybrid diesel-electric multiple unit with optimally sized energy storage system according to the dynamic programming-based control ($\alpha = 0.2$): (a) vehicle speed profile, (b) total requested power and power provided by internal combustion engine and energy storage system, and (c) energy storage system state-of-charge.
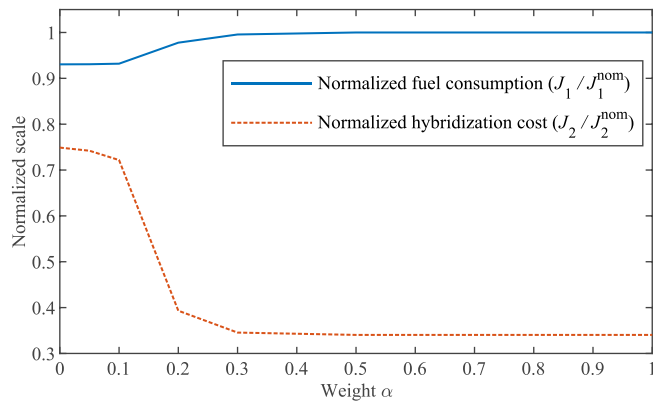
Fig. 13. The trade-off between lower fuel consumption and lower hybridization cost.

4.3.3. Influence **of the control strategy**

The influence of the control strategy on the optimal solution is investigated in this section. For this aim, a causal and implementable rule-based strategy is defined. The flowchart of the rules for this controller is presented in Fig. 14. In order to ensure fulfillment of the main hybridization requirement of emissions-free and noise-free operation during stops, a piecewise lower limit of ESS SoC is introduced, where $\sigma_{\min,stop}$ represents the SoC lower limit during stops, set to a value that satisfies the following condition:

$$n_{par} \cdot n_{ser} \cdot P_{cell,cont,dch}(\sigma_{\min,stop}) \geq P_{elaux}, \tag{37}$$

and $\sigma_{\min,run}$ is the SoC lower limit during motion, set to a value that satisfies the following condition:

$$n_{par} \cdot n_{ser} \cdot \left(E_{cell,max}(\sigma_{\min,run}) - E_{cell,max}(\sigma_{\min,stop})\right) \geq E_{elaux,stop,max}. \tag{38}$$

Since the condition (37) is satisfied for all possible SoC lower limits for all 228 ESS configurations, it is set to $\sigma_{\min,stop} = 10\%$ as in the previous case, while the lover limit during motion is set to $\sigma_{\min,run} = 40\%$. The upper limit remains the same as in the previous case, i.e. $\sigma_{\max} = 90\%$. According to the defined algorithm, during stops ($v = 0$) the ESS provides complete requested power, and the ICE is switched off. If the ESS discharges to $\sigma_{\min,stop}$ before the departure (caused by delayed departure, for instance), the ICE is started and supplies the total demanded power. In case of negative power demand, generally occurring when the vehicle is braking, the braking energy is used for recharging the ESS, and ICE operates with no load. In case of high power demand, in our case set to a value exceeding 60% of the maximum available power from the ICE-G set, the ESS provides maximum available power for supporting the ICE. This typically occurs during vehicle acceleration. For the lower levels of demanded power (i.e., during cruising or coasting phases), the ESS provides support for the ICE limited to the electrical auxiliaries power demand. This operation mode is sustained until $\sigma_{\min,run}$ is reached. Once this occurs, the controller switches to "load level increase" mode, where the ICE provides additional power used for recharging the ESS. In order to prevent frequent switching between ESS charging and

discharging, and at the same time from excessive usage of ICE instead of braking power for charging the ESS, a 5% hysteresis for the SoC is considered during this phase of low power demand.

The same approach for determining the ESS optimal size described in Section 3 is conducted by using the defined RB control instead of DP. Compared to the DP-based control, simulation time for the entire trip with implemented RB control takes less than 2 s on average per feasible ESS configuration. The overall results are given in Table 6. The increase in fuel consumption across α, in this case, is 15.2%, while the total cost of hybridization is reduced by 65.8%. Compared to the standard DMU, fuel savings range from 19.2% for the most fuel-efficient solution down to 7% for the most cost-efficient solution. Regarding the ESS size and configuration, achieving the most fuel-efficient solution, in this case, requires significant ESS size and related cost increase compared to the solution obtained with the implemented DP controller. The differences in results from the two control strategies are emphasized in Fig. 15, where the fuel consumption level for all 228 ESS configurations and related costs is plotted. The fuel consumption is normalized with the results obtained for the standard DMU for overall comparison.

Fig. 16 shows the total requested power split and SoC of optimally sized ESS at a weight $\alpha = 0.2$, which contains $n_{par}^{*} = 2$ parallel branches with $n_{ser}^{*} = 202$ cells per branch. As can be seen, the proposed RB controller ensures fulfillment of the main hybridization requirement imposed by the RU; however, its main drawback is the inability to guarantee the ESS SoC sustenance, caused primarily by its causal nature. The following round trip would start with significantly discharged ESS, considering the given periodic timetable and corresponding vehicle circulation plan. This would result in higher fuel consumption than the given results, thus implying its significant impact and biased input for the primary optimization problem.

Regarding the local pollutants, emissions results are diverse (see Fig. 17). Depending on the ESS size and configuration, simulation results for DMU with DP controller demonstrated a decrease of NO_x emissions ranging from 3.5% up to 11.8% compared to the standard DMU emissions level, while RB control resulted in an increase of 20.3% up to 34.1%. For PM emissions, both controls demonstrated a reduction compared to the standard DMU ranging between 60.3 and 61.2% for DP control and between 14.9 and 21.3% for RB control.

5. Discussion

The detailed analysis presented in the previous section showed significant potential benefits from hybridization of a DMU vehicle. These benefits are reflected primarily in the reduction of fuel consumption and resulting CO_2 emissions, theoretically reaching almost 35% compared to the conventional DMU. Although the focus of this study was on a specific case study in the Netherlands, the presented methodology can be applied to other regional railway networks and DMU vehicles, regardless of the geographical context. In addition, the proposed optimization algorithm allows for fair generalization and relatively easy adaptation to other railway vehicles and types of services. Moreover, straightforward determination of feasible ESS configurations based on existing technologies allows for a direct implementation of the solution.

Table 5
Optimization results for different values of weight α with implemented dynamic programming-based control.

Indicator	Unit	α						
		0	0.05	0.1	0.2	0.3	0.5	1
J^{*}	–	0.9305	0.9213	0.9109	0.8609	0.8006	0.6702	0.3404
J_1	liter	76.4661	76.4852	76.5853	80.3508	81.8187	82.1773	82.1773
J_2	EUR	11235.84	11133.70	10827.26	5898.82	5183.81	5107.20	5107.20
n_{par}^{*}	cell	4	4	4	2	2	2	2
n_{ser}^{*}	cell	220	218	212	231	203	200	200

Fig. 14. Flowchart for the proposed rule-based controller.

Due to its non-causal nature (i.e., assuming perfect information on future driving conditions), frequent switches in ESS control, as well as required computation time (i.e., 3 min on average in this case), the DP-based EMS cannot be directly implemented in a real-time controller. However, having in mind the main aim of this study – determining the optimal size of ESS, which represents a strategic decision, the presented approach identifies ESS parameters that yield the absolute largest potential in reducing fuel consumption, regardless of the EMS in place.

The main advantages of the presented RB controller are its straightforward implementation in real-time energy management, at the same time satisfying the main requirement of providing enough power and energy for supplying auxiliaries during stabling periods. Due to implemented hysteresis, it prevents frequent switches in ESS charging/ discharging, thus improving its life cycle durability. However, the inability to guarantee ESS SoC sustenance and significantly decreased performance compared to the DP controller make the ESS sizing

Table 6

Optimization results for different values of weight α with implemented rule-based control.

Indicator	Unit	α						
		0	0.05	0.1	0.2	0.3	0.5	1
J^*	–	0.8530	0.8602	0.8645	0.8530	0.7893	0.6613	0.3404
J_1	liter	94.2559	94.2559	96.5694	108.3127	108.3127	108.5326	108.5326
J_2	EUR	14938.56	14338.56	11695.49	5158.27	5158.27	5107.20	5107.20
n_{par}^*	cell	5	5	4	2	2	2	2
n_{ser}^*	cell	234	234	229	202	202	200	200
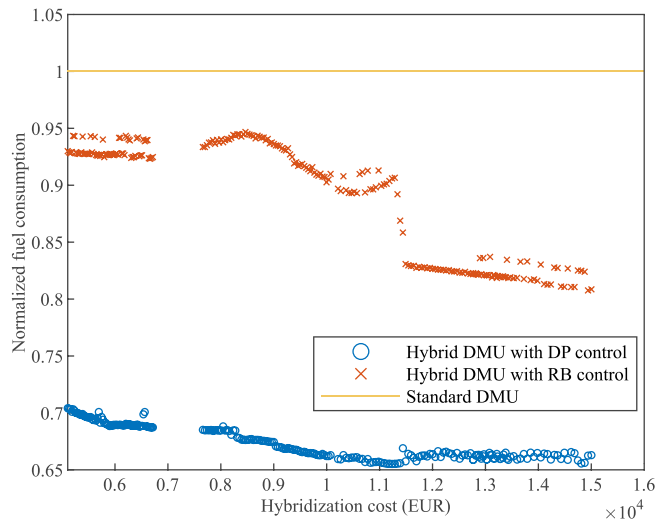
Fig. 15. Relative fuel savings for hybrid diesel-electric multiple unit as a function of energy storage system size and implemented control, compared to the conventional vehicle.

problem obtained with RB control biased.

This research stresses the importance of synthesizing and practical implementation of real-time energy management that would lead to an optimum or near-optimum performance in terms of energy consumption. In this context, DP-based control can be used either to obtain a reference fuel consumption or to obtain optimal power split trajectories that can later be used in defining implementable real-time control strategies. Heuristic RB controls or combining the EFCM method with DP or optimal control theory [94,95] are promising approaches in this regard. The development of such algorithms, coupled with advanced

power management hardware technologies, requires significant effort from the whole industry, and especially from the vehicle manufacturers.

Regarding the local pollutants emissions, results indicate a significant influence of the choice of EMS, with a negative impact on NO$_x$ emissions obtained in case of sub-optimal rule-based control. Even though these emissions are not included in the optimization problem but only as additional indicators, the simulation results with a characteristic mapping of Stage IIIA ICE found in the analyzed vehicle show that hybridization as an instrument could not lead to the fulfillment of Stage IIIB emissions limits. Significant specific reduction requirements imposed by the legislation, especially for PM emissions, reaching almost 90% reduction from Stage IIIA to IIIB, together with the fact that the legislation is focusing only on specific load points of ICE [96], stipulate the necessity of using advanced exhaust ATSs.

6. Conclusions

This paper presented a method to support the decision in the conversion of standard diesel-electric multiple units to their hybrid counterpart by adding an optimally sized Li-ion battery-based energy storage system. The proposed bi-level multi-objective optimization approach based on a nested coordination framework includes relevant design aspects, such as the requirement of achieving emissions-free and noise-free operation in stations, the preference between lower fuel consumption and hybridization cost, technical constraints related to battery voltage and maximum allowed mass, and the influence of the energy management strategy. The case study of selected two-coach diesel multiple unit and railway line demonstrated fuel savings and CO$_2$ emissions reduction ranging between 29.6% and 34.5% with optimal dynamic programming-based control, and from 7% to 19.2% for sub-optimal rule-based control, compared to the conventional vehicle, depending on the ESS size and configuration. At the same time, the implementation of optimal control allowed for preventing ESS oversizing and avoiding
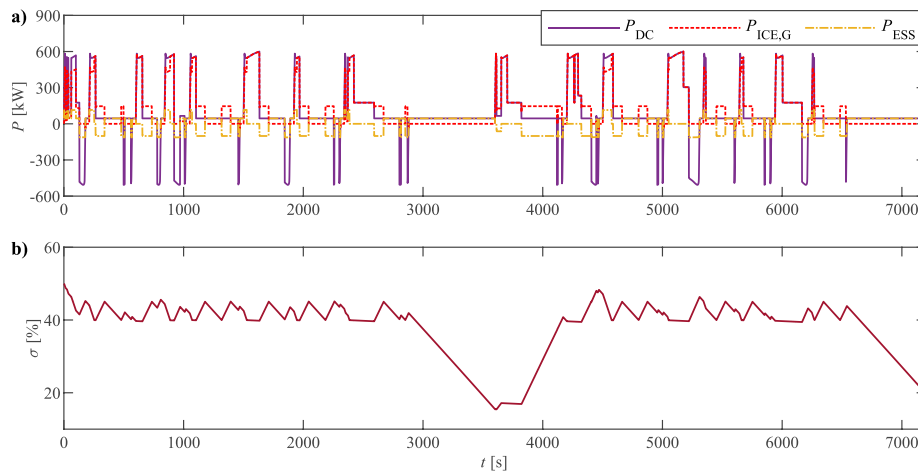

Fig. 16. Simulation results for hybrid diesel-electric multiple unit with optimally sized energy storage system according to the rule-based control ($\alpha = 0.2$): (a) total requested power and power provided by internal combustion engine and energy storage system, and (b) energy storage system state-of-charge.
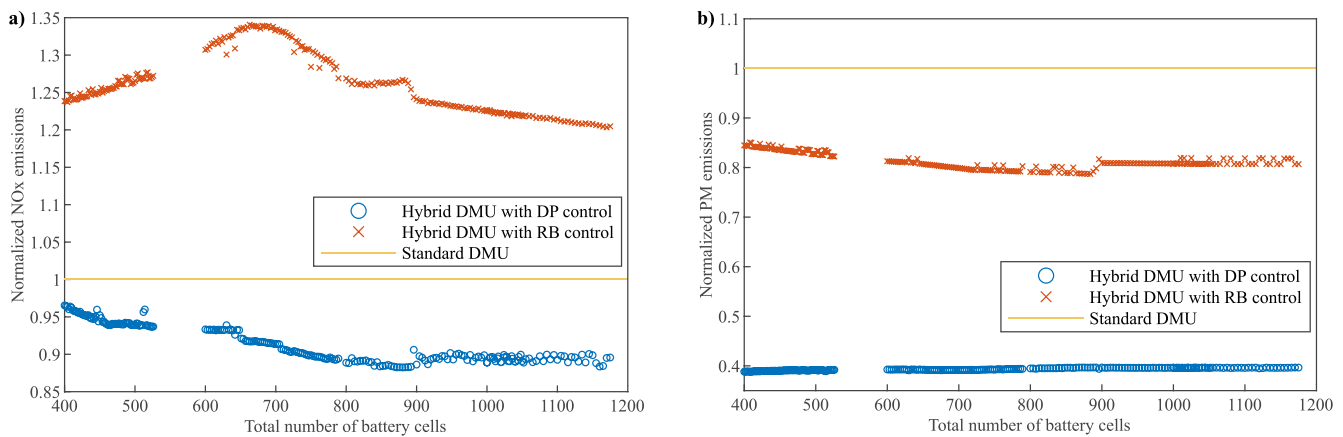
Fig. 17. Normalized local pollutants emissions for standard and hybrid diesel-electric multiple unit depending on the energy storage system size and implemented control: (a) NO$_x$ emissions, and (b) PM emissions.

additional costs. Additionally, a non-linear dependence between hybridization cost and potential fuel savings was identified. The influence of energy management is even more evident in the case of local pollutants, especially NO$_x$ emissions, where the negative impact compared to a standard vehicle is obtained.

The presented research aimed to provide the basis for further developing a wider-scope tool, coined "CO$_2$ Barometer". The aim of the CO$_2$ Barometer is to enable dynamic monitoring and prediction of overall emissions from regional railway services provided on the Northern lines in the Netherlands, and at the same time to offer a decision support tool for the railway undertaking in the analysis of potential future traction options, by capturing the technical innovation and different technological, operational and policy measures. Future applications of the present research will include other types of rolling stock in the fleet, while considering remaining lines and services on the network. Special focus will be on further testing and validation of the proposed method in real-world operation, within the ongoing rolling stock refurbishment program of Arriva. Further extensions to the current work will include the development of a causal control strategy with respect to the system architecture in place that would be able to provide results that converge to the global optimum. Additionally, analysis of other energy storage and propulsion systems based on supercapacitors and hydrogen fuel cells, as well as the environmental impact of using alternative fuels such as hydrotreated vegetable oil will be conducted, while extending the research scope to well-to-wheel and life cycle perspective.

CRediT authorship contribution statement

Marko Kapetanović: Methodology, Software, Validation, Writing - original draft, Writing - review & editing, Visualization. **Alfredo Núñez:** Methodology, Validation, Formal analysis, Investigation, Writing - original draft, Writing - review & editing, Supervision. **Niels van Oort:** Conceptualization, Resources, Writing - original draft, Supervision, Project administration. **Rob M.P. Goverde:** Conceptualization, Methodology, Writing - original draft, Writing - review & editing, Supervision.

Declaration of Competing Interest

The authors declare that they have no known competing financial interests or personal relationships that could have appeared to influence the work reported in this paper.

Acknowledgment

References

[1] UN. Kyoto Protocol to the United Nations Framework Convention on Climate Change. Kyoto; 1998. https://unfccc.int/resource/docs/convkp/kpeng.pdf. [Accessed 8 October 2020].

[2] UN. Paris Agreement. Paris; 2015. https://unfccc.int/sites/default/files/english_paris_agreement.pdf. [Accessed 8 October 2020].

[3] UIC, CER. Moving towards sustainable mobility: A Strategy for 2030 and Beyond for the European Railway Sector. Paris; 2012. http://www.cer.be/sites/default/files/publication/CER-UIC_Sustainable_Mobility_Strategy_-_SUMMARY.pdf. [Accessed 15 September 2020].

[4] Beatrice C, Rispoli N, Di Blasio G, Patrianakos G, Kostoglou M, Konstandopoulos A, et al. Emission Reduction Technologies for the Future Low Emission Rail Diesel Engines: EGR vs SCR. SAE Tech. Pap., vol. 6; 2013. https://doi.org/10.4271/2013-24-0087.

[5] Ding X, Wang Z, Zhang L, Wang C. Longitudinal Vehicle Speed Estimation for Four-Wheel-Independently-Actuated Electric Vehicles Based on Multi-Sensor Fusion. IEEE Trans Veh Technol 2020;69:12797–806. https://doi.org/10.1109/TVT.2020.3026106.

[6] Ding X, Wang Z, Zhang L. Hybrid Control-Based Acceleration Slip Regulation for Four-Wheel-Independently-Actuated Electric Vehicles. IEEE Trans Transp Electrif 2021:1–14. https://doi.org/10.1109/TTE.2020.3048405.

[7] Buzzoni L, Pede G. New prospects for public transport electrification. Electr Syst Aircraft. Railw Sh Propulsion, ESARS 2012:2–6. https://doi.org/10.1109/ESARS.2012.6387464.

[8] Deur J, Škugor B, Cipek M. Integration of Electric Vehicles into Energy and Transport Systems. Automatika 2015;56:395–410. https://doi.org/10.1080/00051144.2015.11828654.

[9] Shakya SR, Shrestha RM. Transport sector electrification in a hydropower resource rich developing country: Energy security, environmental and climate change co-benefits. Energy Sustain Dev 2011;15:147–59. https://doi.org/10.1016/j.esd.2011.04.003.

[10] IEA, UIC. Railway Handbook 2017. Energy Consumption and CO2 Emissions. Focus on Passenger Rail Services; 2017. https://uic.org/IMG/pdf/handbook_iea-uic_2017_web3.pdf. [Accessed 5 September 2020].

[11] Al-Tony FE-S, Lashine A. Cost-benefit analysis of railway electrification: case study for Cairo-Alexandria railway line. Impact Assess Proj Apprais 2000;18:323–33. https://doi.org/10.3152/147154600781767312.

[12] Cambridge Systematics Inc. Final technical memorandum, Task 8.3: Analysis of Freight Rail Electrification in the SCAG Region, prepared for Southern California association of governments; 2012.

[13] Jones H, Moura F, Domingos T. Life cycle assessment of high-speed rail: a case study in Portugal. Int J Life Cycle Assess 2017;22:410–22. https://doi.org/10.1007/s11367-016-1177-7.

[14] Dincer I, Zamfirescu C. A review of novel energy options for clean rail applications. J Nat Gas Sci Eng 2016;28:461–78. https://doi.org/10.1016/j.jngse.2015.12.007.

[15] Meinert M, Melzer M, Kamburow C, Palacin R, Leska M, Aschemann H. Benefits of hybridisation of diesel driven rail vehicles: Energy management strategies and life-cycle costs appraisal. Appl Energy 2015;157:897–904. https://doi.org/10.1016/j.apenergy.2015.05.051.

[16] Meinert M, Prenleloup P, Schmid S, Palacin R. Energy storage technologies and hybrid architectures for specific diesel-driven rail duty cycles: Design and system

integration aspects. Appl Energy 2015;157:619–29. https://doi.org/10.1016/j.apenergy.2015.05.015.

[17] Klebsch W, Heininger P, Martin J. Alternatives to diesel multiple units in regional passenger rail transport: Assessment of systemic potential. Frankfurt Am Main 2019.

[18] Klebsch W, Guckes N, Heininger P. Evaluation of climate-neutral alternatives to diesel multiple units: Economic viability assessment based on the example of the 〉Düren network. Frankfurt Am Main 2020.

[19] Beatrice C, Rispoli N, Di Blasio G, Konstandopoulos AG, Papaioannou E, Imren A. Impact of Emerging Engine and After-Treatment Technologies for Improved Fuel Efficiency and Emission Reduction for the Future Rail Diesel Engines. Emiss Control Sci Technol 2016;2:99–112. https://doi.org/10.1007/s40825-016-0035-1.

[20] Konstandopoulos AG, Kostoglou M, Beatrice C, Di Blasio G, Imren A, Denbratt I. Impact of Combination of EGR, SCR, and DPF Technologies for the Low-Emission Rail Diesel Engines. Emiss Control Sci Technol 2015;1:213–25. https://doi.org/10.1007/s40825-015-0020-0.

[21] Scheepmaker GM, Goverde RMP, Kroon LG. Review of energy-efficient train control and timetabling. Eur J Oper Res 2017;257:355–76. https://doi.org/10.1016/j.ejor.2016.09.044.

[22] Railway Gazette International. Hybrid drive demonstrates 15% fuel saving; 2015. https://www.railwaygazette.com/traction-and-rolling-stock/hybrid-drive-demonstrates-15-fuel-saving/40806.article. [Accessed 2 October 2020].

[23] Fujii T, Teraya H, Osawa M. Special edition paper Development of an NE train. JR EAST Tech Rev 2004:62–70.

[24] Shiraki N, Satou H, Arai S. A hybrid system for diesel railcar series Ki-Ha E200. 2010 Int Power Electron Conf - ECCE ASIA -, IEEE; 2010, p. 2853–8. https://doi.org/10.1109/IPEC.2010.5542319.

[25] Engel B, Soefker C. The innovative traction system with the flywheel of the LIREX™. World Congr Railw Res 2001.

[26] Research and Technology Centre of Deutsche Bahn AG. Applications for energy storage flywheels in vehicles of Deutsche Bahn AG. World Congr Railw Res; 2001.

[27] EC. Public Report: ultra low emission vehicle – transport using advanced propulsion 2 (ULEV-TAP II). Erlangen; 2005.

[28] Marsilla M. CleanER-D Deliverable 7.5.4: Future scenarios and recommendations for implementation of hybrid solutions; 2013.

[29] Hillmansen S, Roberts C, Mcgordon A, Jennings P. Concept Validation for Hybrid Trains. Final Report DfTRG/0078/2007. Birmingham; 2008.

[30] Hillmansen S, Roberts C, Mcgordon A, Jennings P. DMU hybrid concept evaluation. Final Report DfTRG/0078/2007. Birmingham; 2009.

[31] United Nations. Economic Commission for Europe. ECE/TRANS/WP.6/2011/5: Definitions of vehicle energy types. Geneva; 2011.

[32] González-Gil A, Palacin R, Batty P, Powell JP. A systems approach to reduce urban rail energy consumption. Energy Convers Manag 2014;80:509–24. https://doi.org/10.1016/j.enconman.2014.01.060.

[33] González-Gil A, Palacin R, Batty P. Sustainable urban rail systems: Strategies and technologies for optimal management of regenerative braking energy. Energy Convers Manag 2013;75:374–88. https://doi.org/10.1016/j.enconman.2013.06.039.

[34] Boulter PG, McCrae IS. ARTEMIS: Assessment and Reliability of Transport Emission Models and Inventory Systems – Final Report 2007.

[35] Knörr W, Heidt C, Notter B, Läderach A, Biemann K, Antes R. Ecological Transport Information Tool for Worldwide Transports. Methodology and Data, Update 2018; 2018.

[36] Knörr W, Hüttermann R. EcoPassenger: Environmental Methodology and Data. Heidelberg: Hannover; 2016.

[37] Guzzella L, Sciarretta A. Vehicle propulsion systems: Introduction to modeling and optimization. 3rd ed. Berlin: Springer; 2013.

[38] Horrein L, Bouscayrol A, Delarue P, Verhille JN, Mayet C. Forward and backward simulations of a power propulsion system. IFAC; 2012.

[39] Gao DW, Mi C, Emadi A. Modeling and Simulation of Electric and Hybrid Vehicles. Proc IEEE 2007;95:729–45. https://doi.org/10.1109/JPROC.2006.890127.

[40] Fiori C, Ahn K, Rakha HA. Power-based electric vehicle energy consumption model: Model development and validation. Appl Energy 2016;168:257–68. https://doi.org/10.1016/j.apenergy.2016.01.097.

[41] Wang J, Rakha HA. Electric train energy consumption modeling. Appl Energy 2017;193:346–55. https://doi.org/10.1016/j.apenergy.2017.02.058.

[42] Schmid S, Ebrahimi K, Pezouvanis A, Commerell W. Model-based comparison of hybrid propulsion systems for railway diesel multiple units. Int J Rail Transp 2017; 6:16–37. https://doi.org/10.1080/23248378.2017.1390790.

[43] Leska M, Prabel R, Aschemann H, Rauh A. Optimal Operating Strategy for Hybrid Railway Vehicles based on a Sensitivity Analysis. IFAC Proc 2014;47:942–7. https://doi.org/10.3182/20140824-6-ZA-1003.02019.

[44] Leska M, Aschemann H. Fuel-optimal combined driving strategy and energy management for a parallel hybrid electric railway vehicle. 2015 20th Int Conf Methods Model Autom Robot MMAR 2015; 2015. p. 1127–32. https://doi.org/10.1109/MMAR.2015.7284037.

[45] Leska M, Aschemann H, Melzer M, Meinert M. Comparative Calculation of the Fuel-Optimal Operating Strategy for Diesel Hybrid Railway Vehicles. Int J Appl Math Comput Sci 2017;27:323–36. https://doi.org/10.1515/amcs-2017-0023.

[46] Lanneluc C, Pouget J, Poline M, Chauvet F, Gerbaud L. Optimal Energy Management of a Hybrid Train: Focus on Saving Braking Energy. 2017 IEEE Veh Power Propuls Conf, IEEE 2017:1–6. https://doi.org/10.1109/VPPC.2017.8330927.

[47] Poline M, Gerbaud L, Pouget J, Chauvet F. Simultaneous optimization of sizing and energy management — Application to hybrid train. Math Comput Simul 2019;158: 355–74. https://doi.org/10.1016/j.matcom.2018.09.021.

[48] Joud L, Da Silva R, Chrenko D, Kéromnès A, Le Moyne L. Smart Energy Management for Series Hybrid Electric Vehicles Based on Driver Habits Recognition and Prediction. Energies 2020;13:2954. https://doi.org/10.3390/en13112954.

[49] Agbli KS, Hissel D, Sorrentino M, Chauvet F, Pouget J. Reverse engineering of a railcar prototype via energetic macroscopic representation approach. Energy Convers Manag 2016;112:61–80. https://doi.org/10.1016/j.enconman.2015.12.072.

[50] Agbli KS, Devillers N, Chauvet F, Hissel D, Sorrentino M. Energetic Macroscopic Representation in Reverse Engineering Process: Railcar Hybridization. 2016 IEEE Veh Power Propuls Conf, IEEE 2016:1–6. https://doi.org/10.1109/VPPC.2016.7791683.

[51] Mayet C, Mejri M, Bouscayrol A, Pouget J, Riffonneau Y. Energetic Macroscopic Representation and inversion-based control of the traction system of a hybrid locomotive. 2012 IEEE Veh Power Propuls Conf, IEEE 2012:491–6. https://doi.org/10.1109/VPPC.2012.6422763.

[52] Silvas E, Hofman T, Murgovski N, Etman P, Steinbuch M. Review of Optimization Strategies for System-Level Design in Hybrid Electric Vehicles. 1–1 IEEE Trans Veh Technol 2016;66. https://doi.org/10.1109/TVT.2016.2547897.

[53] Spiryagin M, Cole C, Sun YQ, McClanachan M, Spiryagin V, McSweeney T. Design and Simulation of Rail Vehicles. 1st ed. Taylor & Francis Group LLC; 2014.

[54] Sun Y, Cole C, Spiryagin M, Godber T, Hames S, Rasul M. Conceptual designs of hybrid locomotives for application as heavy haul trains on typical track lines. Proc Inst Mech Eng Part F J Rail Rapid Transit 2013;227:439–52. https://doi.org/10.1177/0954409713501655.

[55] Vazquez S, Lukic SM, Galvan E, Franquelo LG, Carrasco JM. Energy storage systems for transport and grid applications. IEEE Trans Ind Electron 2010;57: 3881–95. https://doi.org/10.1109/TIE.2010.2076414.

[56] Ghaviha N, Campillo J, Bohlin M, Dahlquist E. Review of Application of Energy Storage Devices in Railway Transportation. Energy Procedia 2017;105:4561–8. https://doi.org/10.1016/j.egypro.2017.03.980.

[57] Dittus H, Hülsebusch D, Ungethüm J. Reducing DMU fuel consumption by means of hybrid energy storage. Eur Transp Res Rev 2011;3:149–59. https://doi.org/10.1007/s12544-011-0053-6.

[58] Fathy HK, Reyer JA, Papalambros PY, Ulsov AG. On the coupling between the plant and controller optimization problems. In: Proc 2001 Am Control Conf (Cat. No.01CH37148), IEEE, vol.3; 2001. p. 1864–9. https://doi.org/10.1109/ACC.2001.946008.

[59] Sorrentino M, Cirillo V, Nappi L. Development of flexible procedures for co-optimizing design and control of fuel cell hybrid vehicles. Energy Convers Manag 2019;185:537–51. https://doi.org/10.1016/j.enconman.2019.02.009.

[60] Sarma U, Ganguly S. Determination of the component sizing for the PEM fuel cell-battery hybrid energy system for locomotive application using particle swarm optimization. J Energy Storage 2018;19:247–59. https://doi.org/10.1016/j.est.2018.08.008.

[61] Sarma U, Ganguly S. Design optimisation for component sizing using multi-objective particle swarm optimisation and control of PEM fuel cell-battery hybrid energy system for locomotive application. IET Electr Syst Transp 2020;10:52–61. https://doi.org/10.1049/iet-est.2018.5053.

[62] Pisu P, Rizzoni G. A Comparative Study Of Supervisory Control Strategies for Hybrid Electric Vehicles. IEEE Trans Control Syst Technol 2007;15:506–18. https://doi.org/10.1109/TCST.2007.894649.

[63] Sorrentino M, Serge Agbli K, Hissel D, Chauvet F, Letrouve T. Application of dynamic programming to optimal energy management of grid-independent hybrid railcars. 095440972092008 Proc Inst Mech Eng Part F J Rail Rapid Transit 2020. https://doi.org/10.1177/0954409720920080.

[64] Lu S, Hillmansen S, Roberts C. Power management strategy study for a multiple unit train. IET Conf. Railw. Tract. Syst. (RTS 2010), IET; 2010, p. 29–29. https://doi.org/10.1049/ic.2010.0035.

[65] Lu S, Hillmansen S, Roberts C. A Power-Management Strategy for Multiple-Unit Railroad Vehicles. IEEE Trans Veh Technol 2011;60:406–20. https://doi.org/10.1109/TVT.2010.2093911.

[66] García-Garre A, Gabaldón A. Analysis, Evaluation and Simulation of Railway Diesel-Electric and Hybrid Units as Distributed Energy Resources. Appl Sci 2019;9: 3605. https://doi.org/10.3390/app9173605.

[67] Pröhl L. OPEUS Deliverable DO2.1 - OPEUS simulation methodology, EU-project OPEUS (S2R-OC-CCA-02-2015); 2017.

[68] Pröhl L. OPEUS Deliverable DO2.2 - OPEUS simulation tool, EU-project OPEUS (S2R-OC-CCA-02-2015); 2017.

[69] Brünger O, Dahlhaus E. Running time estimation. In: Hansen IA, Pachl J, editors. Railw. Timetabling Oper. Hamburg: Eurailpress; 2014. p. 65–89.

[70] Davis WJ. The tractive resistance of electric locomotives and cars. Gen Electr Rev 1926;29:685–707.

[71] Luan X, Wang Y, De Schutter B, Meng L, Lodewijks G, Corman F. Integration of real-time traffic management and train control for rail networks - Part 2: Extensions towards energy-efficient train operations. Transp Res Part B Methodol 2018;115:72–94. https://doi.org/10.1016/j.trb.2018.06.011.

[72] Vučić V. Public transport (in Serbian). Belgrade: Scientific Book; 1987.

[73] Dinić D. Railway traction (in Serbian). Belgrade: Publishing Institute of Yugoslavian Railways; 1986.

[74] Profillidis VA. Railway Engineering. 2nd ed. Burlington, USA: Ashgate Publishing Company; 2000.

[75] Leska M, Gruning T, Aschemann H, Rauh A. Optimization of the longitudinal dynamics of parallel hybrid railway vehicles. Proc IEEE Int Conf Control Appl 2012:202–7. https://doi.org/10.1109/CCA.2012.6402436.

[76] Prohl L, Aschemann H. Grey Wolf optimisation of an operating strategy for energy storage systems in electrically driven railway vehicles. 2019 18th Eur Control Conf ECC 2019; 2019. p. 1908–13. https://doi.org/10.23919/ECC.2019.8795720.

[77] Ebbesen S, Dönitz C, Guzzella L. Particle swarm optimisation for hybrid electric drive-train sizing. Int J Veh Des 2012;58:181. https://doi.org/10.1504/IJVD.2012.047382.

[78] Cipek M, Pavković D, Kljaić Z, Mlinarić TJ. Assessment of battery-hybrid diesel-electric locomotive fuel savings and emission reduction potentials based on a realistic mountainous rail route. Energy 2019;173:1154–71. https://doi.org/10.1016/j.energy.2019.02.144.

[79] Bellman R. Dynamic Programming. Mineola, NY: Dover Publications; 2003.

[80] Sundström O, Ambühl D, Guzzella L. On Implementation of Dynamic Programming for Optimal Control Problems with Final State Constraints. Oil Gas Sci Technol – Rev l'Institut Français Du Pétrole 2010;65:91–102. https://doi.org/10.2516/ogst/2009020.

[81] Bellman R. On the theory of dynamic programming. Proc Natl Acad Sci USA 1952;38:716–9.

[82] Ghaviha N, Bohlin M, Holmberg C, Dahlquist E, Skoglund R, Jonasson D. A driver advisory system with dynamic losses for passenger electric multiple units. Transp Res Part C Emerg Technol 2017;85:111–30. https://doi.org/10.1016/j.trc.2017.09.010.

[83] Leska M, Gruning T, Aschemann H, Rauh A. Optimal trajectory planning for standard and hybrid railway vehicles with a hydro-mechanic transmission. 2013 Eur Control Conf ECC 2013; 2013. p. 4550–5. https://doi.org/10.23919/ecc.2013.6669576.

[84] Giro Batalla R, Feenstra M. Energy consumption in GTW DMU trains - ECO Driving. Arriva Nederland: Project statement; 2012.

[85] Stadler Bussnang AG. GTW DMU-2 2/6 and GTW 2/8 low-floor for Arriva, Netherlands. n.d. https://www.stadlerrail.com/media/pdf/garr1008e.pdf. [Accessed 4 September 2020].

[86] CleanER-D. Clean European Rail-Diesel. Seventh Framework Programme 7.2.1.1 Sustainable Surface Transport. Project deliverables. 2020. http://www.cleaner-d.eu/deliverables.htm.

[87] Paukert H. CleanER-D Deliverable 7.2.1: Detailed Specification: Parameters definition; 2011.

[88] Pourabdollah M. On Optimization of Plug-in Hybrid Electric Vehicles. Thesis for the degree of licentiate of engineering. Göteborg, Sweden: Chalmers University of Technology; 2012.

[89] Pourabdollah M, Murgovski N, Grauers A, Egardt B. Optimal Sizing of a Parallel PHEV Powertrain. IEEE Trans Veh Technol 2013;62:2469–80. https://doi.org/10.1109/TVT.2013.2240326.

[90] Pourabdollah M, Murgovski N, Grauers A, Egardt B. An iterative dynamic programming/convex optimization procedure for optimal sizing and energy management of PHEVs. IFAC Proc 2014;47:6606–11. https://doi.org/10.3182/20140824-6-ZA-1003.02375.

[91] SAFT. Ion-OnBoard® Regen, the Li-ion regenerative hybrid traction battery system n.d. https://www.saftbatteries.com/products-solutions/products/ion-onboard®-regen-li-ion-regenerative-hybrid-traction-battery-system?page=1 (accessed April 1, 2020).

[92] SAFT, UNEW. OPEUS Deliverable D6.1 - Innovative technologies outlook update. EUproject OPEUS (S2R-OC-CCA-02-2015); 2017.

[93] Sundstrom O, Guzzella L. A generic dynamic programming Matlab function. 2009 IEEE Int Conf Control Appl, IEEE 2009:1625–30. https://doi.org/10.1109/CCA.2009.5281131.

[94] Ambuhl D, Guzzella L. Predictive Reference Signal Generator for Hybrid Electric Vehicles. IEEE Trans Veh Technol 2009;58:4730–40. https://doi.org/10.1109/TVT.2009.2027709.

[95] Nazari S, Middleton R, Siegel J, Stefanopoulou A. Equivalent Consumption Minimization Strategy for a Power Split Supercharger. WCX SAE World Congr. Exp. 2019. https://doi.org/10.4271/2019-01-1207.

[96] DieselNet. ISO 8178 2020. https://dieselnet.com/standards/cycles/iso8178.php.